## REMARKS

Applicant is submitting herewith a Request for Continued Examination (RCE), pursuant to 37 C.F.R. §1.114, together with the requisite fee of $790.00 provided for under 37 C.F.R. §1.17(e). Accordingly, Applicant respectfully submits that the "final" status of the pending Office Action has now been lifted, toward enabling entry and consideration of the present Communication after Final Action.

Applicant again advises the Examiner of a change in the prosecuting attorneys for this case. Applicant is in the process of obtaining execution of the requisite Revocation and Substitute Power of Attorney, and Statement under 37 C.F.R. §3.73(b) forms, expressly naming the undersigned firm and designated attorneys as Applicant's representatives for this case. In the interim, Applicant respectfully requests acceptance and entry of the present Amendment and Communication, on the basis of Applicant's undersigned attorneys' apparent authority, as evidenced by possession of the file enabling preparation of the instant response to the pending Office Action.

Claims 1 - 22 have been rejected under 35 U.S.C. §103(a) as being unpatentable over Funakawa et al., US 6,666,932. Specifically, the Examiner has stated that Example 2 of Funakawa (as exemplified at Tables 3 and 4 of that reference) discloses specific examples which meet or "closely approximate" the composition limitations of Applicant's claims, and that Applicant's claimed process steps do not patentably distinguish its claims over Funakawa. Applicant respectfully traverses the Examiner's substantive bases for rejection of the claims.

Applicant respectfully submits that its claims 1-22 are patentably distinguishable over the cited Funakawa reference on at least two bases. First, the Examiner has not addressed the issue of whether Example 2 of Funakawa discloses a steel having a two-phase microstructure comprising about 30% polygonal ferrite and about 70% acicular ferrite, as required by subpart (b) of each of Applicant's independent claims 1, 10, 14 and 18. Example 2 of Funakawa neither teaches nor discloses a steel having such a two-phase microstructure. To the contrary, Example 2 of Funakawa teaches that each of the steel sheets 1 to 10, identified as being examples of the invention, had a microstructure identified as "ferrite structure single phase" (Col. 10, lines 56-60) (emphasis added). Moreover, Funakawa's "Summary of the Invention" clearly teaches that the object of the invention is achieved only by a steel sheet "consisting essentially of a matrix of ferrite structure single phase" (Col. 2, lines 1-6) (emphasis added). In the "Detailed Description of the Invention", Funakawa clearly states that the object of the present invention can only be achieved by a steel having a ferrite single phase in the amount of 95% or more:

> In the present invention, the ferrite structure single phase need not always consist of a 100% ferrite phase. If the ferrite phase is 95% or more, the object of the present invention can be achieved. (Col. 3, lines 34-37).

Applicant respectfully submits that one of ordinary skill in the art would define Applicant's claimed microstructure comprising about 30% polygonal ferrite and about 70% acicular ferrite as a two-phase microstructure, rather than the single phase microstructure described by Funakawa. Applicant has submitted herewith a copy of an article from ISIJ (Iron and Steel Institute of Japan) International, Vol. 42 (2002), entitled "Effect of Microstructure on the Yield Ratio and Low Temperature Toughness of Linepipe Steels", by Y.M. Kim, S.M. Kim, Y.J. Lim and N.J. Kim. In the Abstract of that article, the authors describe how they investigated several two-phase steel alloy systems to determine the effects of microstructural features on the yield ratio and toughness of certain steels. At p. 1572, col. 2, the authors identify one of those two-phase steel alloys as comprising "acicular ferrite steels with polygonal ferrite as second phase" (emphasis added). Applicant has also submitted herewith a copy of an article from the November 2002 *Welding Journal* entitled "Microstructural Variations in a High-Strength Structural Steel Weld under Isoheat Input Conditions", by B. Basu and R. Raman, in which the authors clearly indicate that polygonal ferrite and acicular ferrite are considered to be distinct structures having different physical characteristics, and which in combination do not comprise a "single phase". For example, at p. 244, col. 3, the authors describe how, upon cooling, austenite transforms to a variety of different microstructures, including grain boundary ferrite, ferrite side plates, polygonal ferrite and acicular ferrite, at different transformation starting temperatures.

Thus, it is clear that Funakawa, which discloses only single-phase ferrite steels, neither teaches nor suggests Applicant's claimed two-phase microstructure comprising about 30% polygonal ferrite and about 70% acicular ferrite, as required by subpart (b) of Applicant's independent claims 1, 10, 14 and 18. As such, Applicant respectfully submits that each of its independent claims 1, 10, 14 and 18 patentably distinguishes over the cited Funakawa reference.

Second, the Examiner has stated that an average grain size of no more than 5 microns, as required by subpart (b) of each of Applicant's independent claims 1, 10, 14 and 18, "would be expected since compositional and other microstructural limitations are met, and in absence of proof to the contrary." Applicant respectfully submits that the Examiner has failed to state a *prima facie* case that the average grain size limitation of Applicant's claims would be obvious to one of skill in the art in view of Funakawa. Indeed, the Examiner has admitted that Funakawa does not teach that a fine ferrite grain size of less than 5 microns would be expected, and points to no teaching or suggestion in any prior art reference which teaches or suggests an average grain size of less than 5 microns. Thus, Applicant respectfully submits that the Examiner has failed to state a *prima facie* case that one of ordinary skill in the art, in making a steel using Applicant's claimed composition and process steps, would necessarily obtain a two-phase microstructure having an average grain size of no more than about 5 microns.

Moreover, Applicant respectfully submits that the Examiner's position is misplaced, in view of the fact that Funakawa actually teaches away from a steel having an average grain size of less than 5 microns. Funakawa teaches that one of the objects of the invention is to provide a hot rolled steel sheet having high elongation (Col. 1, lines 23-27). Among the prior art references discussed in the "Background of the Invention" section of Funakawa is JP-A-11-152544, which is indicated as disclosing a steel sheet in which the grain size of ferrite is controlled to be as fine as 2 microns or smaller (Col. 1, lines 55-59). Rather than indicate that such a fine ferrite grain size is desirable, however, Funakawa indicates the opposite, by stating that high elongation (one of the objects of the invention) cannot be obtained by the prior art because of the fine ferrite grain size of 2 microns or smaller. Moreover, Funakawa does not teach that an average ferrite grain size of greater than 2 microns but less than 5 microns would be expected or desirable. Accordingly, Funakawa teaches away from a fine ferrite grain size of 5 microns or less. Thus, Applicant respectfully submits that the Examiner's reliance on

Funakawa likewise fails to state a *prima facie* case that Applicant's claimed average grain size of 5 microns or less would be obvious to one of ordinary skill in the art.

In view of the foregoing, Applicant respectfully submits that its independent claims 1, 10, 14 and 18 are not obviated by the Funakawa reference cited by the Examiner, whether taken alone or in combination with other, unspecified prior art. Specifically, Applicant respectfully submits that Funakawa neither teaches nor suggests the specific compositions set forth in elements a - c of each of claims 1, 10, 14 and 18, in combination with the important process steps of elements d - f, of each respective one of claims 1, 10, 14 and 18. Therefore, Applicant respectfully submits that each of amended independent claims 1, 10, 14 and 18 patentably distinguishes over Funakawa.

Accordingly, reconsideration and withdrawal of the rejections of claims 1, 10, 14 and 18, and allowance of independent claims 1, 10, 14 and 18, are all respectfully solicited.

Inasmuch as dependent claims 2 - 8, 11 - 13, 15 - 17 and 19 - 22 merely serve to further define the subject matter of independent claims 1, 10, 14 and 18, respectively, dependent claims 2 - 8, 11 - 13, 15 - 17 and 19 - 22 likewise should be deemed to patentably distinguish over the cited Funakawa reference. Accordingly, reconsideration and withdrawal of the rejections of dependent claims 2 - 8, 11 - 13, 15 - 17 and 19 - 22, and allowance thereof, are likewise respectfully solicited.

Applicant submits that the application as a whole, including all of claims 1 - 22, is now in condition for allowance. Reconsideration and allowance of the application as a whole, are therefore respectfully solicited.

Should anything further be required, a telephone call to the undersigned, at (312) 456-8400, is respectfully invited.

Respectfully submitted,

Dated: May 3, 2006

Jeffrey P. Dunning
One of Attorneys for Applicant

## CERTIFICATE OF MAILING

I hereby certify that this correspondence is being deposited with the United States Postal Service as First Class Mail on the date set forth below, pursuant to 37 C.F.R. §1.8, in an envelope addressed to: Mail Stop RCE, Commissioner for Patents, P.O. Box 1450, Alexandria, VA 22313-1450.

Dated: May 3, 2006

Jeffrey P. Dunning

ISIJ International, Vol. 42 (2002), No. 12, pp. 1571–1577

# Effect of Microstructure on the Yield Ratio and Low Temperature Toughness of Linepipe Steels

Y. M. KIM, S. K. KIM,[1] Y. J. LIM[2] and N. J. KIM

Department of Materials Science and Engineering and Center for Advanced Aerospace Materials, Pohang University of Science and Technology, Pohang 790-784, Korea. 1) POSLab, Gwangyang, Korea. 2) Quality Technology Dept. POSCO, Pohang, 790-360 Korea.

*(Received on May 22, 2002; accepted in final form on September 29, 2002)*

The present study aims at elucidating the effects of microstructural features on the yield ratio and toughness of high strength linepipe steels. The main emphasis has been placed on understanding the effects of constituents on the properties. Several alloy systems with different constituents, *i.e.* ferrite–pearlite steels, ferrite steels with acicular ferrite as second phase, acicular ferrite steels with ferrite as second phase, and bainite steels, have been investigated. Experimental results show that while the refinement of ferrite grain size improves both yield strength and low temperature toughness of ferrite-base steels, it increases the yield ratio. Modification of matrix from ferrite to acicular ferrite or bainite results in improvements in both yield strength and yield ratio. However, bainite steels have worse low temperature toughness (*i.e.*, higher DBTT) than the other types of steels. It has been shown that the low temperature toughness of acicular ferrite steels can be improved by the introduction of polygonal ferrite as a second phase. This is mainly due to the refinement of effective grain size by the introduction of second phases. The relationship between the yield ratio and work hardening exponent has also been established using the Swift equation. Based on the results, the optimum microstructure for a better combination of strength, toughness and yield ratio is suggested to be the one having second phase of polygonal ferrite in an acicular ferrite or bainite matrix.

KEY WORDS: steel; DBTT; yield ratio; toughness.

## 1. Introduction

Linepipe steels, which transport oil and gas, should have high strength, high toughness, excellent corrosion resistance and superior weldability.[1-3] The current demand is towards the larger-diameter and higher-pressure linepipes to improve the efficiency of transmission, resulting in more stringent specifications for the linepipe steels. In addition to the above mentioned properties, the steels should have low yield ratio (yield strength/tensile strength) for the safety concern. The lower yield ratio means the higher resistance to deformation from yielding to plastic instability,[4,5] preventing the sudden decrease in the strength. According to the engineering specifications, API X-70 steels should have the yield strength higher than 480 MPa, impact energy larger than 100 J at −40°C and the yield ratio smaller than 85%. It has been shown in the previous study that the achievement of low yield ratio (around 80%) and high toughness (ductile–brittle transition temperature of around −100°C) is possible in the 440 MPa grade C–Mn steel by controlling the thermomechanical process.[6] However, it becomes more difficult to maintain adequate values of yield ratio and toughness as strength increases to a higher level. The basic difficulty in optimizing these properties comes from the fact they are often inversely correlated, *i.e.* an increase in the strength is achieved at the expense of the yield ratio and toughness, and *vice versa*. Therefore to develop the high performance linepipe steels, the individual effect of microstructural features on these properties should be clearly understood.

One of the ways of decreasing the yield ratio is the utilization of hard second phase in the microstructure. Numerous studies on so-called dual phase steels showed that these steels have low yield ratio due to the presence of hard martensite or bainite in soft ferrite matrix.[7,8] Shikanai *et al.*,[9] analyzed the relationship between the volume fraction and morphology of second phase and the yield ratio by finite element method (FEM) and reported that the steel should have soft matrix with around 50% volume fraction of hard second phase to obtain low yield ratio. It has also been suggested that the larger difference in the strength between the two phases is more desirable to obtain low yield ratio.[9,10] However these dual phase steels generally have low yield strengths which do not meet the property requirement for X-70 linepipe steels. Moreover the large difference in the strength between the two phases might have a deleterious effect on toughness since cracks can easily nucleate at the hard second phase particles at low temperatures. Recently, more emphasis is placed on developing acicular ferrite or bainite base steels for linepipe applications.[11-13] However, the toughness of these steels is often disappointing. Therefore new microstructures are needed to obtain the adequate combinations of strength, toughness and yield ratio.

© 2002 ISIJ

**Table 1.** Chemical compositions of the steels used in the present study (mass%).

| Steel | C | Mn | Si | Cr | Mo | Ni | Nb | Ti | P | S | B |
|---|---|---|---|---|---|---|---|---|---|---|---|
| A | 0.08 | 1.51 | 0.20 | - | - | - | 0.05 | 0.02 | 0.002 | 0.003 | - |
| B | 0.06 | 1.22 | 0.26 | - | - | - | 0.05 | 0.02 | 0.004 | 0.003 | - |
| C | 0.06 | 1.22 | 0.26 | - | 0.29 | - | 0.05 | 0.02 | 0.004 | 0.003 | - |
| D | 0.06 | 1.21 | 0.26 | - | 0.47 | - | 0.05 | 0.02 | 0.004 | 0.003 | - |
| E | 0.06 | 1.24 | 0.26 | 0.19 | 0.30 | 0.62 | 0.05 | 0.02 | 0.004 | 0.003 | - |
| F | 0.06 | 1.20 | 0.26 | - | 0.47 | - | 0.05 | 0.02 | 0.004 | 0.003 | 0.0015 |
| G | 0.02 | 1.55 | 0.16 | - | 0.49 | 0.21 | 0.05 | 0.02 | 0.002 | 0.003 | 0.0025 |

**Table 2.** Rolling conditions used for the production of the steels.

<table>
<tr><td>Rolling condition</td><td colspan="9">70mm $\xrightarrow{\text{Pass 1}}$ 51mm(27.1%) $\xrightarrow{\text{Pass 2}}$ 43mm(15.7%) $\xrightarrow{\text{Pass 3}}$ 37mm(14%) $\xrightarrow{\text{Pass 4}}$ 31mm(16.2%) $\xrightarrow{\text{Pass 5}}$ 27mm(12.9%) $\xrightarrow{\text{Pass 6}}$ 23mm(12.6%) $\xrightarrow{\text{Pass 7}}$ 20mm(15.3%)</td></tr>
<tr><td>Steel</td><td>Pass 1 (°C)</td><td>Pass 2 (°C)</td><td>Pass 3 (°C)</td><td>Pass 4 (°C)</td><td>Pass 5 (°C)</td><td>Pass 6 (°C)</td><td>FRT (°C)</td><td>CT (°C)</td><td>CR (°C/s)</td></tr>
<tr><td>A1</td><td rowspan="3">1150</td><td rowspan="3">1100</td><td rowspan="3">1050</td><td rowspan="3">950</td><td rowspan="3">930</td><td rowspan="3">890</td><td>870</td><td>670</td><td>26</td></tr>
<tr><td>A4</td><td>870</td><td>600</td><td>37</td></tr>
<tr><td>A5</td><td>870</td><td>530</td><td>33</td></tr>
<tr><td>A2</td><td rowspan="2">1150</td><td rowspan="2">1100</td><td rowspan="2">1050</td><td rowspan="2">950</td><td rowspan="2">920</td><td rowspan="2">870</td><td>750</td><td>600</td><td>12</td></tr>
<tr><td>A3</td><td>750</td><td>530</td><td>15</td></tr>
<tr><td>Rolling condition</td><td colspan="9">70mm $\xrightarrow{1150°C}$ 60mm(14.3%) $\xrightarrow{1050°C}$ 50mm(16.7%) $\xrightarrow{900°C}$ 42mm(16%) $\xrightarrow{850°C}$ 30mm(28.6%) $\xrightarrow{845°C}$ 20mm(33.3%) $\xrightarrow{830°C}$ 13mm(35%)</td></tr>
<tr><td>Steel</td><td colspan="3">FRT (°C)</td><td colspan="3">CT (°C)</td><td colspan="3">CR (°C/s)</td></tr>
<tr><td>B, C, D, E, F</td><td colspan="3" rowspan="4">830</td><td colspan="3">580</td><td colspan="3">15</td></tr>
<tr><td>G1</td><td colspan="3" rowspan="3">450</td><td colspan="3">4</td></tr>
<tr><td>G2</td><td colspan="3">11</td></tr>
<tr><td>G3</td><td colspan="3">17</td></tr>
</table>

* FRT : finish rolling temperature, CT : coiling temperature, CR : cooling rate

The objective of the present study is to elucidate the effects of microstructural features on yield ratio and toughness of high strength linepipe steels. Of particular interest is the effect of constituents. Several alloy systems with different microstructural constituents, *i.e.* ferrite–pearlite steels, ferrite steels with acicular ferrite as second phase, acicular ferrite steels with polygonal ferrite as second phase, and bainite steels, have been chosen for this study.

## 2. Experimental Procedure

Chemical compositions of the steels used in the present study are shown in **Table 1**. These steels were produced in a laboratory scale and subjected to various rolling conditions to produce various microstructures.[14–16] Details of rolling procedures are shown in **Table 2**. Specimen blanks for tensile specimens were cut from the rolled plates in the transverse direction. Tensile specimens were round bars with 6 mm gage diameter and 30 mm gage length. Tensile tests were conducted at room temperature with a cross head speed of 9 mm/min. Yield strength of the steels showing discontinuous yielding behavior was taken at the lower yield point, while that of the other steels was taken at 0.2% offset. Reported tensile properties are the averages of at least 3 test results. Charpy V notch impact specimens (JIS No. 4) were also cut from the rolled plate in the transverse direction. Specimens were tested at temperatures ranging from −120 to 20°C with 20°C intervals after soaking for 15 min in the bath controlled by liquid nitrogen and alcohol. Ductile–brittle transition temperature (DBTT) was taken as the temperature corresponding to the mid-point of the upper and lower shelf energies. Fracture surfaces of broken Charpy specimens were examined using scanning electron microscopy (SEM). Volume fraction of the constituent phases and the grain size were analyzed by using an image analyzer.

## 3. Results

### 3.1. Microstructure

**Figure 1** shows the representative microstructures of the steels with various constituents. These are ferrite–pearlite steels (Fig. 1(a)), ferrite steels with acicular ferrite as second phase (Fig. 1(b)), acicular ferrite steels with polygonal ferrite as second phase (Fig. 1(c)), and bainite steels (Fig. 1(d)).

Detailed microstructural characteristics of the steels are summarized in **Table 3**. Ferrite grain size of the ferrite–pearlite steels ranges from 6.8 to 20.4 $\mu$m. The volume fraction of acicular ferrite in the ferrite–acicular ferrite steels varies from 9.6 to 24.1%. The ferrite–acicular ferrite steels also contain a small amount of pearlite (around 2%). The ferrite grain sizes of the ferrite–acicular ferrite steels ranges from 4.4 to 7.4 $\mu$m, which is generally finer than those of the ferrite–pearlite steels. The acicular ferrite–ferrite steels are characterized by the presence of fine (around 4.5 $\mu$m) polygonal ferrite grains within the elongated acicular ferrite matrix. The volume fraction of ferrite in the acic-

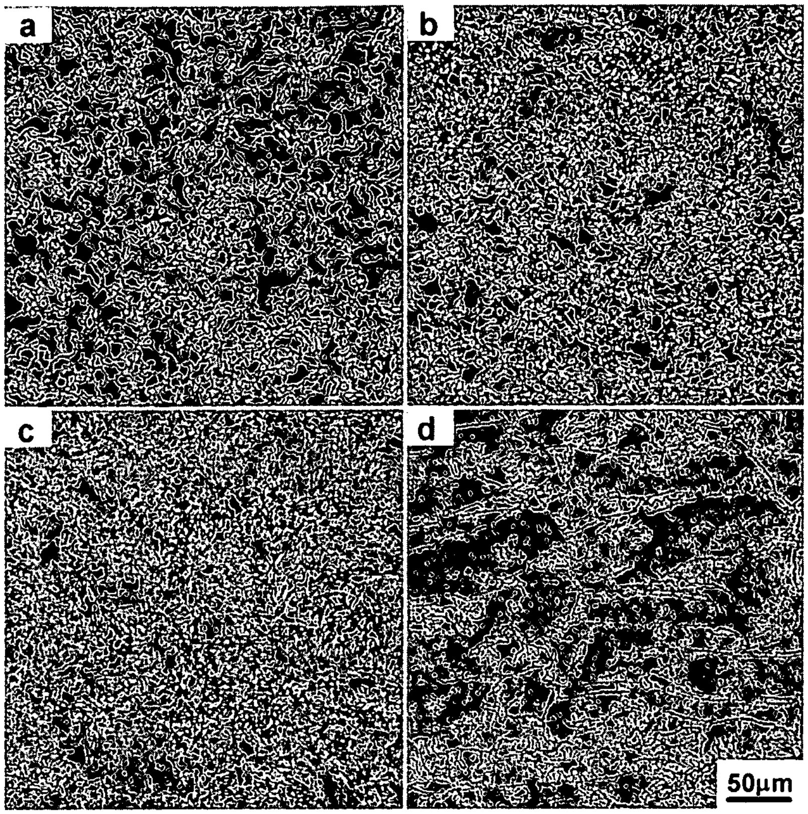

**Fig. 1.** Representative microstructures of the steels with various constituents; (a) ferrite–pearlite steel (B steel), (b) ferrite steel with acicular ferrite as second phase (C steel), (c) acicular ferrite steel with polygonal ferrite as second phase (D steel), and (d) bainite steel (G2 steel).

**Table 3.** Details of microstructural features of various steels.

| Structure | Steel | Ferrite Grain Size (μm) | Vol. % of Second Phase | | |
|---|---|---|---|---|---|
| | | | Ferrite (%) | Pearlite (%) | AF or B (%) |
| F-P | A1 | 9.6 | 90.7 | 9.3 | - |
| | A2 | 20.4 | 91.2 | 8.8 | - |
| | A3 | 11.8 | 93.0 | 5.2 | 1.8 |
| | B | 6.8 | 98.3 | 1.7 | - |
| F-AF | A4 | 7.4 | 80.5 | 8.1 | 11.4 |
| | A5 | 7.2 | 75.9 | - | 24.1 |
| | C | 4.3 | 88.7 | 1.7 | 9.6 |
| AF-F | D | 4.6 | 5.9 | 2.1 | 92 |
| | E | 4.2 | 5.5 | 1.1 | 93.4 |
| | F | - | - | 2.2 | 97.8 |
| B | G1 | - | 3.0 | - | 97.0 |
| | G2 | - | 2.1 | - | 97.9 |
| | G3 | - | 1.8 | - | 98.2 |

F : ferrite, AF : acicular ferrite, P : pearlite, B : bainite

ular ferrite–ferrite steels is around 6% and the inter-ferrite spacing along the rolling direction is measured to be around 16 μm. The bainite steels have the microstructure consisting of elongated grains, which resemble the morphology of prior austenite grains.

### 3.2. Tensile Properties

Tensile properties of the steels are listed in **Table 4** along with their impact properties. It shows that the bainite steels have the highest strength followed by the acicular ferrite–ferrite steels, the ferrite–acicular ferrite steels and the ferrite–pearlite steels. The strength of multiphase steels is dependent on the volume fraction and strength of constituent phases as shown in previous studies.[7–9] Bainite contains a large amount of dislocations in the microstructure, which causes significant strengthening effect. Therefore, the strength of the bainite steels is the highest, while that of the ferrite–pearlite steel is the lowest. The yielding behavior changes from discontinuous yielding in ferrite–pearlite steels to quasi-continuous yielding in ferrite–acicular ferrite steels. Acicular ferrite–ferrite and bainite steels show continuous yielding behavior.

**Figure 2** shows the relationship between yield strength and yield ratio of the steels. It shows that, at the same yield strength level, the bainite steels have the lowest value of yield ratio, followed by the acicular ferrite–ferrite steels, ferrite–acicular ferrite steels, and the ferrite–pearlite steels. It can also be seen in Fig. 2 that it is very difficult for the ferrite–pearlite steels to meet the tensile property specifications for X-70 grade steels (*i.e.*, yield strength higher than 480 MPa and yield ratio lower than 85%). However, other types of steels can meet the specifications.

### 3.3. Impact Toughness and Fracture Behavior

DBTTs and upper shelf energies of various steels are shown in Table 4. **Figure 3** shows the relationship between yield strength and DBTT of the steels. As is the case of ten-

© 2002 ISIJ

Table 4. Tensile and impact properties of various steels.

| Steel | YS (MPa) | UTS (MPa) | EL (%) | YR (%) | DBTT (°C) | Upper Shelf Energy (J) |
|---|---|---|---|---|---|---|
| A1 | 465 | 555 | 42.5 | 83.8 | -51 | 406 |
| A2 | 458 | 553 | 40.5 | 82.9 | -15 | 400 |
| A3 | 456 | 550 | 37.2 | 82.9 | -31 | 400 |
| B | 469 | 523 | 31.2 | 89.5 | -82 | 421 |
| A4 | 489 | 583 | 35.0 | 83.9 | -40 | 371 |
| A5 | 508 | 582 | 36.5 | 87.3 | -25 | 349 |
| C | 543 | 618 | 25.4 | 87.9 | -79 | 305 |
| D | 587 | 707 | 23.7 | 83.0 | -78 | 266 |
| E | 592 | 719 | 24.2 | 82.5 | -90 | 212 |
| F | 588 | 697 | 19.2 | 84.4 | -63 | 179 |
| G1 | 575 | 718 | 15.3 | 80.2 | -28 | 272 |
| G2 | 629 | 747 | 14.7 | 84.2 | -12 | 255 |
| G3 | 653 | 757 | 11.8 | 86.2 | 3 | 258 |

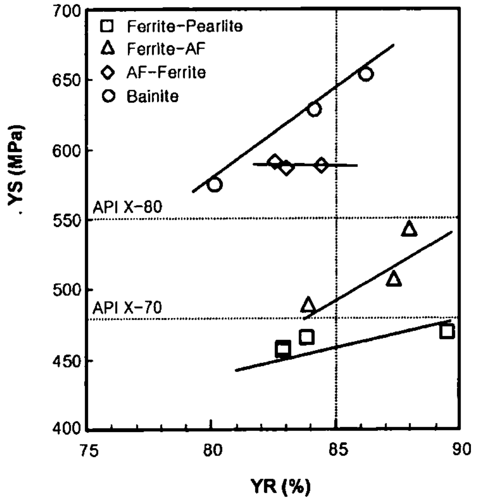

Fig. 2. Relationship between yield strength and yield ratio of various steels.

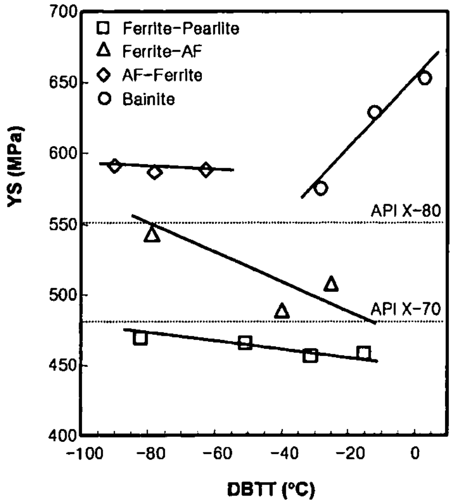

Fig. 3. Relationship between yield strength and DBTT of various steels.

sile properties, it is difficult to make clear analyses on the effect of microstructure on the variation of DBTT since the steels have large differences in the chemical composition. However, there are rather distinctive differences in DBTTs among various microstructures, which clearly shows the effect of microstructure on DBTT. It shows that the acicular ferrite–ferrite steels have the best combinations of yield strength and DBTT. Although bainite steels have very high strength, they have poor low temperature toughness. Their DBTTs range from 3 to −28°C, which are much higher than the property requirement for X-70 grade API steels. Moreover, these steels have much lower shelf energies at all test temperatures than the other types of steels.

Representative SEM fractographs of the steels with various microstructures are shown in **Fig. 4**. Fractographs were taken from the specimens broken at below the respective DBTTs and hence all fractographs show the cleavage fracture surface. As expected from the impact properties, fracture surface shows large differences in the size of cleavage facets depending on the microstructure. It shows that the ferrite-base, *i.e.*, ferrite–pearlite and ferrite–acicular ferrite, steels have the cleavage facets on the scale of ferrite grain size, which is the smallest among all the steels (Fig. 4(a)). The bainite steels have the largest cleavage facets on the scale of prior austenite grain size along the elongated direction (Fig. 4(d)).

## 4. Discussion

### 4.1. Yield Ratio

As shown above, the steels show different combinations of yield strength and yield ratio depending on their microstructural constituents. In general, it can be said that the steel with lower yield strength has the lower value of yield ratio. However, such statement may lead to a wrong conclusion since yield ratio is a function of not only yield strength but also work hardening rate. In the case of ferrite–pearlite steels, reducing the ferrite grain size increases the yield strength with an accompanying increase in yield ratio. Moreover, reducing the ferrite grain size decreases the work hardening rate, which has an additional effect on increasing yield ratio. Similar behavior is operating in the steels having a second phase of acicular ferrite instead of pearlite. However, modification of matrix from ferrite to acicular

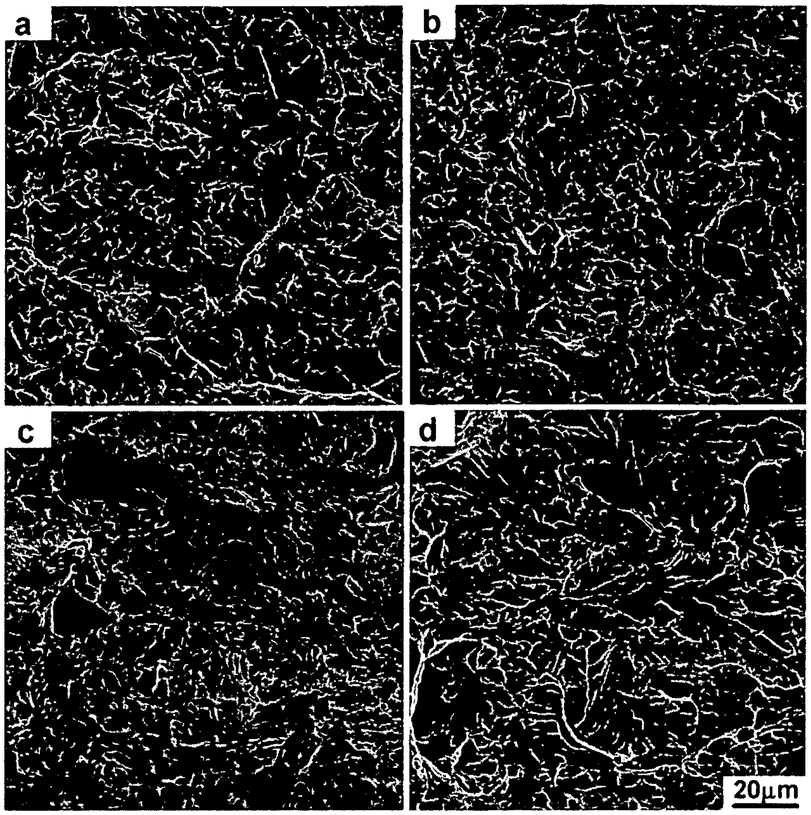

**Fig. 4.** SEM fractographs of broken Charpy impact specimens; (a) ferrite–pearlite steel (B steel), (b) ferrite–acicular ferrite steel (C steel), (c) acicular ferrite–ferrite steel (D steel), and (d) bainite steel (G2 steel).

ferrite results in increase in yield strength and decrease in yield ratio. The existence of large density of mobile dislocations in the acicular ferrite results in continuous yielding and high work hardening rate.[17] When the load is applied, acicular ferrite matrix shows a large response to strain hardening, resulting in a high ultimate tensile strength. The net result is that the steels with acicular ferrite matrix can have lower values of yield ratio than the steels with polygonal ferrite matrix. The steels with bainite matrix have even higher work hardening rate than those with acicular ferrite matrix. Therefore. The bainite-base steels can have lower yield ratio than the acicular ferrite-base steels at the same strength level.

As discussed above, it is impossible to make a general statement on which microstructure has the lowest value of yield ratio since yield ratio is actually a function of both yield strength and work hardening rate. To have a better understanding of the effect of the microstructure on yield ratio, stress–strain behavior of the steels has been analyzed using the Holloman equation and the Swift equation.[14,15] It has been shown that the Holloman equation cannot describe the stress–strain behavior of steels since it underestimates the strength at low strain levels. However, the Swift equation can adequately describe the stress–strain behavior of steels and the relationship between the yield ratio and work hardening exponent has been derived as follows[14,15];

$$\mathrm{YR}=\frac{S_y}{S_u}=\frac{(b+\ln(1+e_y))^N}{(1+e_y)}\,\frac{\exp(N-b)}{N^N} \quad \text{.......(1)}$$

**Table 5.** Values of $b$ in Swift equation and critical work hardening exponent ($N^*$) for achieving the yield ratio of 0.85.

| Structure | b | $N^*$ |
|---|---|---|
| Ferrite-Pearlite | 0.03 | 0.1738 |
| Ferrite-Acicular Ferrite | 0.03 | 0.1738 |
| Acicula Ferrite-Ferrite | 0.01 | 0.1175 |
| Bainite | 0.002 | 0.0796 |

where $S_y$ is the yield strength, $S_u$ is the ultimate tensile strength, $b$ is the additive strain constant, $e_y$ is the engineering strain at yield strength (usually 0.002), and $N$ is the work hardening exponent.

The linear relationship has been established between $\ln(\sigma)$ and $\ln(\varepsilon_p+b)$ by setting the appropriate values of $b$ for each type of microstructure ($\sigma$ is the true stress and $\varepsilon_p$ is the true plastic strain). **Table 5** shows the values of $b$ for each type of microstructure. The values of $b$ range from 0.002 to 0.03, depending on the microstructure with the lowest value of $b$ associated with heavily dislocated structure. It suggests that $b$, the additive strain constant, is a function of amount of strain hardening (*e.g.*, dislocation density) the alloy has received prior to tensile testing. **Figure 5** shows the relationship between the yield ratio and work hardening exponent of various steels. The experimental results agree well with the results calculated using the above equation. It shows that the ferrite-base steels have larger work hardening exponents than the acicular ferrite-

© 2002 ISIJ

or bainite-base steels. Increasing the ferrite grain size increases the work hardening exponent of the ferrite-base steels, thereby decreasing the yield ratio. In the case of acicular ferrite-base steels, increasing the volume fraction of soft second phase of polygonal ferrite increases the work hardening exponents, resulting in a decrease in yield ratio. Comparing the relationship between yield ratio and work hardening exponent of the steels with similar microstructure, it shows that increasing the work hardening exponent decreases the yield ratio. However, the dependence of yield ratio with work hardening exponent varies depending on the type of structure. The steels having higher work hardening rate (*e.g.*, bainite-base steels) have lower yield ratio than the steels having lower work hardening rate (*e.g.*, ferrite-base steels) when compared at the same value of work hardening exponent. The critical work hardening exponent ($N^*$) for achieving the yield ratio of 0.85 is also shown in Table 5. It can be seen that $N^*$ is the lowest for the bainite-base steels, followed by the acicular ferrite-base, and the ferrite-base steels.

## 4.2. Low Temperature Toughness

As shown in Fig. 4, the sizes of the cleavage facets are different depending on the microstructural constituents, with the smallest in ferrite-base steels and the largest in the bainite steels. It suggests that the effective grain sizes controlling DBTT are also different depending on the microstructural constituents. In the case of ferrite-base steels, the effective grain size is the ferrite grain size. This is confirmed by the cross sectional micrography of the broken Charpy impact specimen (**Fig. 6**(a)) showing the change of crack propagation direction at the ferrite grain boundaries. It is well known that decreasing the ferrite grain size improves both strength and low temperature impact toughness. It can be seen in Fig. 3 that DBTT decreases from −15 to −82°C with refining the ferrite grain size from 20.4 to 6.8 μm.

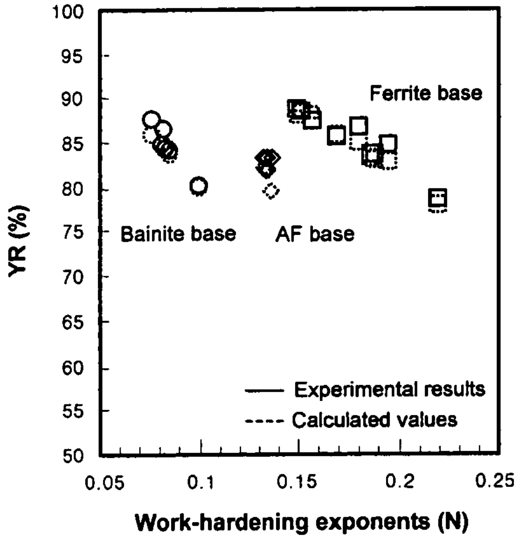

**Fig. 5.** Relationship between yield ratio and work hardening exponent of various steels.

The size of the cleavage facets in bainite steels is very large. In fact, their size is about 100 μm along the direction of crack propagation, which is similar to the diameter of prior austenite grains along elongated direction. This suggests that the effective grain size for the bainite steels is the prior austenite grain size. Cross sectional micrography of the broken Charpy impact specimen (Fig. 6(b)) shows that the crack propagates across the packet boundaries without changing direction, indicating that packet size is not the effective grain size for bainite steels. Although there can be several bainite packets within a prior austenite grain, packet boundaries cannot act as a barrier to cleavage crack propagation since packet boundary is low angle boundary.[16] Moreover, electron back-scatter diffraction (EBSD) analyses show the bainite packets within an austenite grains share the common cleavage planes.[16] The similar behavior has been found in full acicular ferrite steels.[15]

Although the acicular ferrite steels have high DBTTs, incorporation of polygonal ferrite as a second phase can considerably decreases the DBTTs as shown in Fig. 3. Fractography shows that the size of the cleavage facets in the acicular ferrite–ferrite steels is much smaller than that in the bainite steels (Fig. 4). The size of the cleavage facets in the acicular ferrite–ferrite steels is around 22 μm, which is similar to the inter-ferrite spacing. Cross sectional micrography of the broken Charpy impact specimen (Fig. 6(c)) shows that the crack changes its direction when it meets the acicular ferrite/ferrite boundaries (marked by arrow), indicating that the acicular ferrite/ferrite boundaries are the effective barriers to cleavage crack propagation. As in the case of acicular ferrite or bainite steels, packet boundaries do not act as barriers to cleavage crack propagation. Therefore, the effective grain size for the acicular ferrite–ferrite steels is inter-ferrite spacing. Mechanisms of

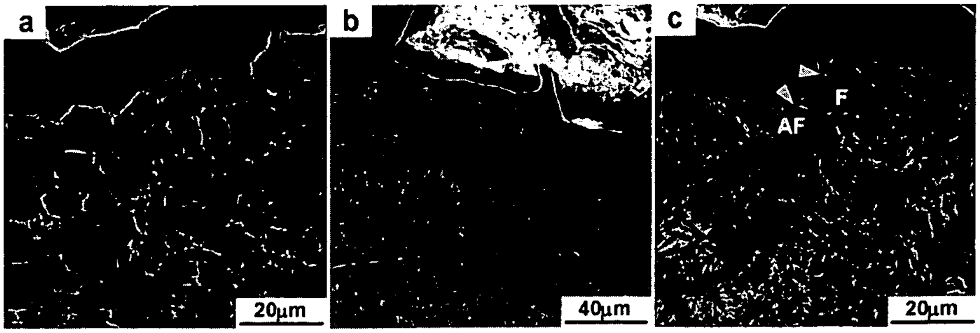

**Fig. 6.** Cross-sectional SEM micrography of the broken Charpy impact specimens; (a) ferrite–pearlite steel (B steel), (b) bainite steel (G2 steel), and (c) acicular ferrite–ferrite steel (D steel).

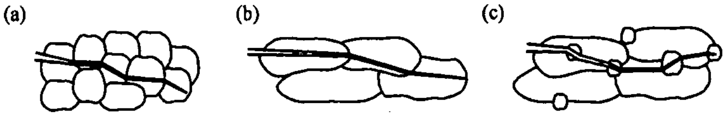

Fig. 7. Schematic drawings showing the cleavage crack propagation in various steels; (a) ferrite-base steel, (b) bainite steel, and (c) acicular ferrite–ferrite steel.

cleavage crack propagation in various steels are schematically shown in **Fig. 7**.

Based on the correlation of microstructure and mechanical properties, optimum microstructure for the development of high performance linepipe steels can be suggested to be the one having second phase of polygonal ferrite in an acicular ferrite or bainite matrix. The achievement of optimum combination of strength, yield ratio and DBTT is difficult in ferrite-base steels since the most effective method for improving strength and toughness, *i.e.*, grain refinement, leads to the increase in yield ratio. On the other hand, acicular ferrite- or bainite-base steels have the advantage of higher yield strength and lower yield ratio over ferrite-base steels. The problem of poor low temperature toughness of these acicular ferrite- or bainite-base steels can be overcome by the introduction of polygonal ferrite as second phase, which reduces the effective grain size.

## 5. Summary

In the present study, the effect of microstructural features on the yield ratio and toughness of high strength linepipe steels have been investigated and the results can be summarized as follows;

(1) While the refinement of ferrite grain size is quite beneficial to the improvement of both yield strength and low temperature toughness of ferrite-base steels, it has an adverse effect on yield ratio in that it increases the yield ratio.

(2) The modification of second phase from pearlite to acicular ferrite or bainite in ferrite-base steels results in the improvement in strength without affecting DBTT. However, acceptable yield ratio has been obtained in the ferrite–acicular ferrite steels only at their lower end of strength.

(3) The modification of matrix phase from ferrite to acicular ferrite or bainite results in the improvement in strength and yield ratio. However, these steels have worse low temperature toughness (*i.e.*, higher DBTT) than the other types of steels due to their much larger effective grain size.

(4) The introduction of polygonal ferrite as a second phase in acicular ferrite or bainite matrix considerably improves the low temperature toughness of acicular ferrite- or bainite-base steels without degrading strength and yield ratio. This is mainly due to the refinement of effective grain size by the introduction of second phase particles.

(5) The relationship between the yield ratio and work hardening exponent has been made. It shows that the dependence of yield ratio with work hardening exponent varies depending on the type of structure. The critical work hardening exponent for achieving the yield ratio of 0.85 is the lowest for the bainite-base structure, followed by the acicular ferrite-base, and the ferrite-base structure.

## REFERENCES

1) N. J. Kim: *J. Met.*, **35** (1983), 21.
2) B. L. Jones and D. L. Johnson: Proc. of an Int. Conf. Steels for Line Pipe and Pipeline Fittings, Metals Society, London, (1981), 14.
3) F. C. Kroft, W. R. Kuntz, W. T. Barrett and B. Nilson: Micro Alloying 75, Union Carbide Corp., New York, (1979), 32.
4) H. Kawamura and B. Kato: Proc. of 2nd Pacific Structural Steel Conf., Australian Institute of Steel Construction, Gold Coast, (1989), 429.
5) Y. Fukumoto: *Eng. Struct.*, **18** (1996),786.
6) N. J. Kim and G. Thomas: *Mater. Sci. Technol.*, **1** (1985) 32.
7) N. J. Kim and G. Thomas: *Metall. Trans.*, **12A** (1981), 483.
8) N. J. Kim and G. Thomas: *Scr. Metall.*, **18** (1984), 817.
9) N. Shikanai, H. Kagawa and M. Kurihara: *ISIJ Int.*, **32** (1992), 335.
10) H. Fischmeister, J.-O. Hjalmered, B. Karlsson, G. Linden and B. Sundstron: The Microstructure and Design of Alloys, Inst. of Metals and Iron & Steel Inst., London, (1973), 621
11) A. B. Cota, R. Barbosa and D. B. Santos: *J. Mater. Process. Technol.*, **106** (2000), 156.
12) A. K. Lis: *J. Mater. Process. Technol.*, **106** (2000), 212.
13) P. C. M. Rodrigues, E. V. Pereloma and D. B. Santos: *Mater. Sci. Eng.*, **283A** (2000), 136.
14) S. K. Kim, Y. J. Lim, Y. M. Kim and N. J. Kim: submitted to *Met. Mater. Int.*
15) S. K. Kim, Y. M. Kim, Y. J. Lim and N. J. Kim: Proc. of 15th Conf. on Mechanical Behaviors of Materials, Korean Institute of Metals and Materials, Seoul, (2001), 177.
16) Y. M. Kim, S. K. Kim and N. J. Kim: "Effect of hot rolling conditions on the tensile and impact properties of ultra low carbon bainitic steels", submitted to *Metall. Mater. Trans.*
17) A. C. Bannister, J. Ruiz Ocejo and F. Gutierrez-Solana: *Eng. Fract. Mech.*, **67** (2000), 547.

© 2002 ISIJ

# Microstructural Variations in a High-Strength Structural Steel Weld under Isoheat Input Conditions

*Weld bead morphologies influence weld cooling rate and hence the acicular ferrite content in steel*

BY B. BASU AND R. RAMAN

ABSTRACT. Bead-in-groove submerged arc welding of quenched and tempered (Q & T) HSLA steel using a suitable welding wire and an agglomerated basic flux (basicity index = 3.1) was carried out under heat input conditions varying from 1.9 to 3.7 kJ/mm. The heat input was adjusted by varying the welding current and welding speed with the machine operated in the constant voltage mode (32–33 VDC). From several welds prepared using a range of currents (400–800 A) and speeds (3–13 mm/s), nine welds were selected. These welds represented those prepared under isoheat input conditions with different current and speed combinations. It was found all the parameters (namely, prior austenitic grain size, inclusion characteristics, cooling rate) influencing the volume fraction of intragranularly precipitated acicular ferrite in the weld showed significantly different dependence at a particular heat input depending upon the welding current and speed combination used. A new cooling rate parameter (NA/C1) based on the weld nugget cross-sectional area (NA) and the fusion zone/heat-affected zone interface length (C1) were defined. Using multiple regression analysis, a correlation between acicular ferrite content and the different influencing parameters as mentioned above was defined having ~90% correlation coefficient. This correlation can be utilized in setting up the trial welding parameters for similar grades of steel substrates and consumables with an aim to maximizing the acicular ferrite content.

## Introduction

In the use of high-strength steels for structural applications, the greatest concern is achievement of the desired mechanical properties in the weld, particularly low-temperature toughness. To economically achieve the required combination of high strength and excellent low temperature toughness in welds for constructional applications, appropriate selection of welding parameters must be addressed. It is a common practice to correlate the various weld metal properties with heat input. Thus, the effects of individual welding parameters such as current and speed are not properly assessed when combined in the form of heat input. The effects of variation of welding current and speed are expected to result in subtle variations in microstructure leading to mechanical properties anywhere between highly desirable to highly deleterious, even though welding might have been carried out using the same heat input. Published information (Refs. 1–4) is available in a very general manner on the effect of welding parameters, particularly heat input, on the structure and properties of high-strength steel welds. However, the effects of individual welding parameters, like current and speed, on the various microstructural and mechanical properties have hardly been systematically addressed, particularly under isoheat input conditions.

It is well established that weld microstructure containing intragranularly formed acicular ferrite, due to its fine basket-weave-like structure, helps to achieve good low-temperature toughness (Refs. 5–8). Extent of formation of such a structure is a result of competition with undesirable higher temperature ferrite morphologies and involves the complex interaction between welding parameters, plate and welding wire chemistry, flux composition, and, significantly, the actual cooling rate the weld experiences. Using the classical approach (Ref. 9) of heat flow in fusion welding, it is possible to estimate the cooling rate experienced by the weld. However, these estimates are rarely accurate, especially with respect to the fusion zone. This is because these empirical equations do not take into account the weld nugget macromorphology that is expected to play a decisive role in the weld cooling rate. Further, the macromorphologies of the weld nugget are expected to depend on the individual welding parameters and cannot be accurately correlated with heat input. In this work, an attempt has been made to study microstructural variations in a submerged arc weld of a high-strength steel under different isoheat input conditions.

KEY WORDS

Submerged Arc Welding
HSLA Steel
Isoheat Input Conditions
Acicular Ferrite
Grain Boundary Ferrite
Polygonal Ferrite
Ferrite Side Plate
CCT Diagram

## Experimental

The objective of the present work is to study the effects of heat input, as a whole, and individual welding parameters such as welding current and speed, under isoheat input conditions, on the microstructural variations of as-deposited weld metal obtained by single-pass, bead-in-groove welding. The single-pass, bead-in-groove welds were characterized for chemistry including oxygen, volume fraction of various microstructural phases, sizes of prior austenitic grains, and inclusion characteristics.

### Materials

**Base plate** — A 22-mm-thick HSLA steel was used for the experiment.

**Welding Wire** — A 3.15-mm-diameter, copper-coated alloyed wire was used as welding wire. Chemical analysis of the base plate and the welding wire used in the experiments is shown in Table 1.

**Flux** — A highly basic, commercially available agglomerated flux with basicity 3.1 was used to carry out the welding. To drive away the moisture absorbed during stor-

---

*B. BASU is Scientist, Naval Materials Research Laboratory, Naval Dockyard, Mumbai, India. R. RAMAN is Professor, Metallurgical Engineering and Materials Science Department, Indian Institute of Technology - Bombay, Mumbai, India.*

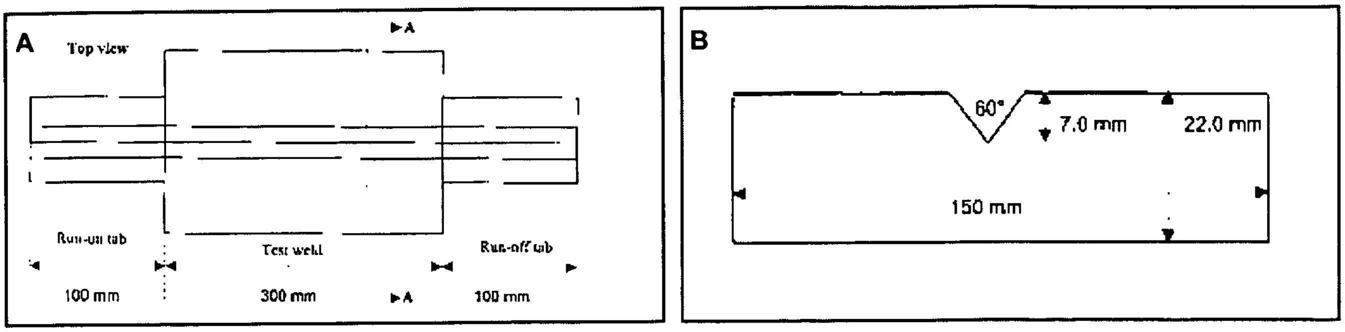

*Fig. 1 — Schematic of the joint geometry. A — Top view; B — side view (section AA).*

**Table 1 — Chemical Composition (wt-%) of Base Metal and Welding Wire**

| Elements | C | Si | Mn | Ni | Cr | Mo | S | P | Cu |
|---|---|---|---|---|---|---|---|---|---|
| Base Metal | 0.08 | 0.23 | 0.4 | 1.8 | 0.44 | 0.29 | <0.01 | <0.01 | 0.38 |
| Welding Wire | 0.04 | 0.1 | 0.81 | 2.6 | 0.07 | 0.24 | <0.01 | <0.01 | 0.11 |

**Table 2 — Chemical Composition of Flux**

| Constituents | $MgO$ | $CaF_2$ | $SiO_2$ | $Al_2O_3$ | $TiO_2$ | $MnO$ | $CaO$ |
|---|---|---|---|---|---|---|---|
| Wt-% | 36 | 26 | 13 | 12 | 0.5 | 0.5 | 12 |

**Table 3 — Welding Parameters**

| Code | Current (Amp) | Speed (mm/s) | Heat Input (kJ/mm) |
|---|---|---|---|
| E | 425 | 7.00 | 1.97 |
| F | 425 | 4.75 | 2.91 |
| G | 425 | 3.70 | 3.73 |
| I | 625 | 10.83 | 1.87 |
| D | 625 | 7.00 | 2.90 |
| C | 625 | 5.45 | 3.72 |
| H | 800 | 13.90 | 1.87 |
| J | 800 | 8.90 | 2.92 |
| K | 800 | 7.00 | 3.71 |

age, the flux was heated in a drying oven at 350°C for 2 h just before use. The approximate composition of the flux constituents is shown in Table 2.

### Weld Preparation

**Joint Geometry** — The plates were ground to a bright metal finish before depositing the beads. Single-pass, bead-in-groove welds were made on 22-mm-thick, 360- x 150-mm steel plates using submerged arc welding (SAW). A SAW machine in constant voltage mode carried out the welding. The joint geometry used for carrying out the test welds is shown in Fig. 1. The run-on tabs allowed enough time to adjust welding current and voltage, while the run-off tabs prevented crater formation within the actual weld of interest. Thus, for each deposit, 300-mm-long deposits of acceptable quality could be achieved.

**Welding Parameters** — A series of submerged arc welds was produced using a range of heat inputs from 2 to 4 kJ/mm at varying current levels from 425 to 800 A. Since a large amount of mechanical, metallurgical, and chemical characterization work was to be done, nine welds were selected from a number of experimental welds. The basis for selection was to include as wide a range of welding speeds as possible. The nine welds selected for analysis represented three heat input levels at three current levels, as illustrated in Table 3. This selection made it possible to study the properties of various welds under isoheat input conditions but with different combinations of individual welding parameters, specifically current and speed. Submerged arc welding was performed using direct current, electrode positive with an initial electrode extension of 22 mm, under constant voltage. Welding voltage was kept constant at 32–33 V for all welding trials.

### Characterization of the Welds

The prepared welds were separated from the run-on and run-off tabs. The separated welds were used for chemical elemental analysis including oxygen content, quantitative metallography, inclusion characteristics, and weld bead morphology.

**Chemical Analysis** — Chemical composition of the as-received base plate and core wire were obtained using an emission spectrometer for the elements manganese, silicon, nickel, chromium, copper, vanadium, and phosphorus and using an interstitial combustion analyzer for carbon and sulfur. Oxygen and nitrogen analysis of the samples was carried out using an infrared oxygen analyzer. The samples for oxygen and nitrogen analysis were taken from the center of the welds and carefully machined using a cooling solution into small cylindrical specimens 2 mm in diameter and 5 mm in length. The chemical analysis, including oxygen, was the average of three results.

**Quantitative Metallography** — Quantitative metallography was carried out using an inverted microscope attached with an image analyzer. The experimental welds were sectioned transverse as well as inclined to the welding direction for metallographic examination, as shown in Fig. 2. Sectioning of the samples for quantitative metallography was done near the middle of the length of the weldment, at two different locations. Due to distortion during sectioning, the measurement on a transverse section may not give the true prior austenitic grain size. Therefore, inclined sections, perpendicular to the columnar grains, were prepared and approximately equiaxed austenite grains were observed and measured. The size of the prior austenite grains was measured by tracing along individual grains and measuring the enclosed area using a computerized image analyzer. More than 100 prior austenite grains were measured from 5 to 10 different fields for all the individual welds. The specimens were mechanically polished to a 0.25-$\mu$ diamond finish in an

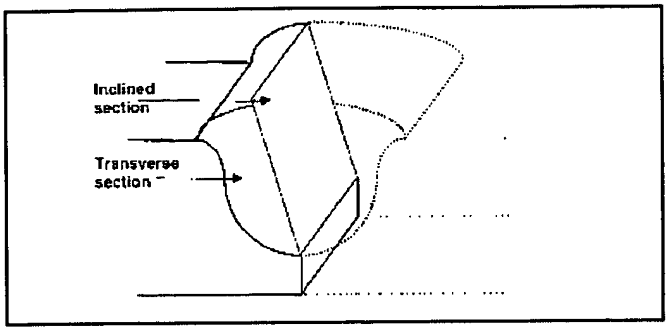

*Fig. 2 — Schematic showing the sample preparation for microstructural characterization. (Inclined section — prior austenitic grain size determination; transverse section — microstructural observation.*

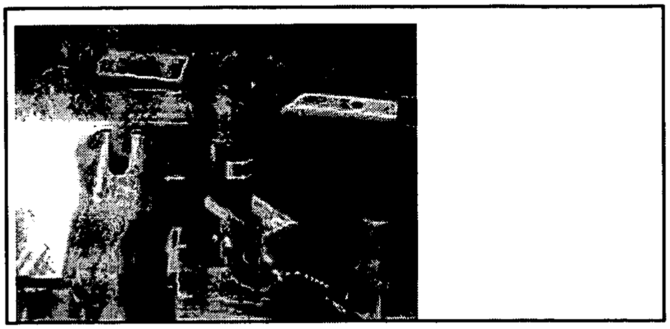

*Fig. 3 — Schematic of weld bead showing different bead morphologies.*

**Table 4 — Chemical Composition of Experimental Welds**

| Code | C | Mn | Si | S | P | Ni | Cr | Mo | Cu | O (ppm) | N (ppm) | $P_{cm}$ |
|---|---|---|---|---|---|---|---|---|---|---|---|---|
| E | 0.077 | 0.77 | 0.22 | 0.009 | 0.020 | 2.47 | 0.24 | 0.25 | 0.47 | 394 | 146 | 0.216 |
| F | 0.055 | 0.77 | 0.21 | 0.006 | 0.020 | 2.60 | 0.23 | 0.25 | 0.47 | 335 | 117 | 0.195 |
| G | 0.054 | 0.78 | 0.19 | 0.007 | 0.023 | 2.41 | 0.22 | 0.25 | 0.45 | 378 | 130 | 0.189 |
| I | 0.070 | 0.76 | 0.22 | 0.005 | 0.021 | 2.50 | 0.25 | 0.26 | 0.51 | 454 | 127 | 0.212 |
| D | 0.064 | 0.73 | 0.23 | 0.006 | 0.019 | 2.47 | 0.26 | 0.25 | 0.49 | 404 | 124 | 0.203 |
| C | 0.063 | 0.75 | 0.24 | 0.006 | 0.020 | 2.46 | 0.24 | 0.25 | 0.49 | 340 | 136 | 0.203 |
| H | 0.075 | 0.77 | 0.25 | 0.005 | 0.016 | 2.31 | 0.24 | 0.25 | 0.50 | 457 | 161 | 0.214 |
| J | 0.065 | 0.77 | 0.23 | 0.005 | 0.018 | 2.61 | 0.27 | 0.26 | 0.45 | 403 | 126 | 0.208 |
| K | 0.064 | 0.77 | 0.22 | 0.005 | 0.018 | 2.63 | 0.24 | 0.25 | 0.47 | 383 | 140 | 0.206 |

automatic polisher. The weld metal microstructure was revealed by etching with a freshly prepared 2% nital solution. The volume fraction of different microstructural constituents, namely, grain boundary ferrite (GBF), polygonal ferrite (PF), ferrite side plate (FSP), and acicular ferrite (AF), were obtained from more than 500 point counts carried out at a magnification of 500X on a transverse section.

**Inclusion Analysis** — Measurement of volume fraction of nonmetallic weld metal inclusions was carried out on transverse sections of the welds. The polished samples were observed without etching at 1500X magnification under an optical microscope attached with an image analyzer. More than 500 inclusions from various fields were taken for quantitative analysis. Due to limitations in the accuracy of detection levels of the optical microscope, inclusions having a diameter of less than 0.20 $\mu$ were not considered for analysis.

**Weld Nugget Morphology** — The morphology of the weld nuggets was measured from samples in the direction transverse to the welding direction. Sectioning of the samples was done at the center of the length of the weld nuggets. Nugget morphologies were measured by tracing an enlarged (10X) image of the polished and macroetched section of the weld profile using a profile projector. The various nugget morphologies measured, as per the schematic of weld bead dimensions shown in Fig. 3, were nugget area (NA) mm$^2$ and fusion zone boundary length (C1) mm.

## Results

### Weld Chemical Analysis

The chemical compositions of the experimental welds are given in Table 4.

### Weld Bead Morphology

The weld nugget morphologies have been tabulated in Table 5. It is assumed the weld nugget cross section is the same throughout the weld length. Hence, the nugget area (NA) (considering unit length of weld) can be assumed to represent the amount of metal fused and the amount of heat to be extracted by the surrounding base metal. In SAW, the cooling of the weld essentially takes place due to the surrounding base metal and, therefore, the fusion zone/HAZ boundary length (C1) (again considering unit length of weld) can be assumed to represent the area through which the heat is transferred. It has been observed that with an increase in current, at each of the three heat input levels, the nugget area increases — Fig. 4. The fusion zone boundary length (C1) was observed to increase with current at all heat input levels (Fig. 5) except at the highest current and highest heat input combination.

### Prior Austenite Grain Size (g)

The variations in austenitic grain sizes (g) with current under isoheat input conditions are listed in Table 5 and shown in Fig. 6. It should be noted the values given are the average of about 100 measurements from different fields done on each weld. Typical micrographs with clearly delineated prior austenite grains are shown in Fig. 7A–C.

### Volume Fraction of Various Phases

Classification of various phases present in the weld was done by IIW method, based on the recommendations of Abson and Pargeter (Ref. 10). The different phases identified and quantified were acicular ferrite, grain boundary ferrite, polygonal ferrite, and ferrite side plates. From the results (Table 6), it can be seen the volume fraction of AF, in general, is quite high and varied between 67 and 84%. It is interesting to note (Fig. 8) that acicular ferrite content shows significant differences in dependence on the welding current although heat input remains the same. This is particularly so at higher levels of welding current at which the weld bead morphology is likely to change significantly due to increased penetration. This is likely to affect cooling rate significantly, as will be explained later, and, hence, AF content. The microstructures showing various phases of the welds are shown in Fig. 9A–C.

### Inclusion Analysis

Inclusion analysis was done using an optical microscope coupled to an image

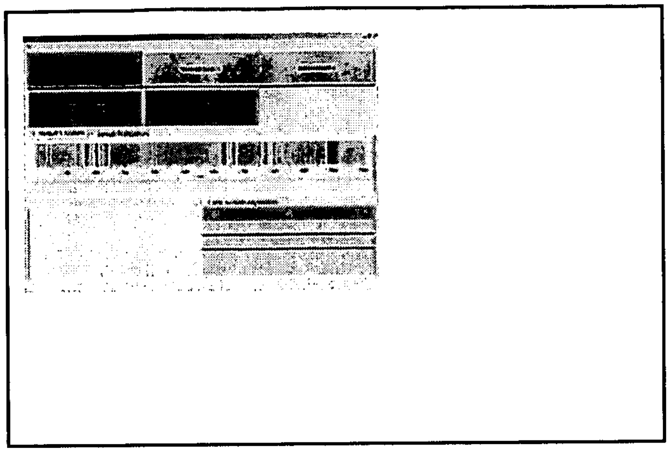

Fig. 4 — *Variation of nugget area with current under isoheat input conditions.*

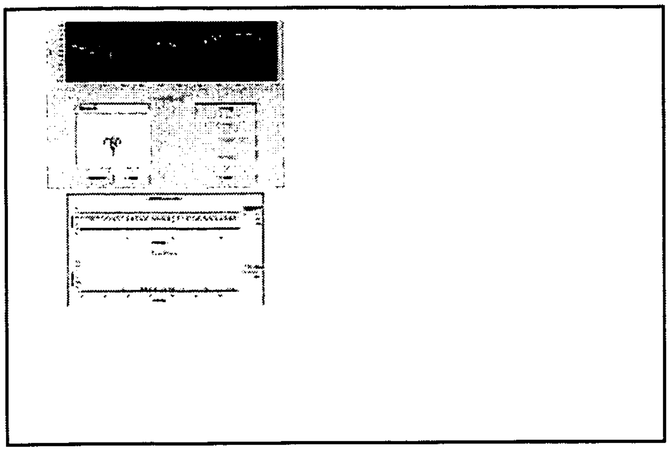

Fig. 5 — *Variation of fusion zone boundary length (C1) with current under isoheat input conditions.*

**Table 5 — Bead Morphology and Prior Austenite Grain Size of Experimental Welds**

| Code | Nugget Area NA ($mm^2$) | Fusion Zone Boundary Length C1 (mm) | Grain Size (μ) |
|---|---|---|---|
| E | 72.4 | 22.1 | 99.3 |
| F | 102.0 | 26.7 | 130.0 |
| G | 120.2 | 28.2 | 155.5 |
| I | 80.6 | 25.2 | 95.0 |
| D | 124.0 | 27.6 | 135.7 |
| C | 177.5 | 34.8 | 146.9 |
| H | 100.8 | 26.5 | 89.0 |
| J | 127.0 | 30.5 | 110.0 |
| K | 181.4 | 32.3 | 132.0 |

**Table 6 — Volume Fraction of Various Microstructural Phases and Inclusion Analysis in Experimental welds**

| Code | Volume fraction of various phases (%) AF | GBF | PF | FSP | Inclusion Size (3-D), dv(μ) | Volume Percent (3-D), f(%) |
|---|---|---|---|---|---|---|
| E | 77.6 | 17.2 | 1.6 | 3.6 | 0.495 | 0.00146 |
| F | 70.6 | 22.6 | 2.0 | 4.8 | 0.504 | 0.00148 |
| G | 67.0 | 27.2 | 1.0 | 4.8 | 0.547 | 0.00229 |
| I | 73.8 | 19.1 | 3.1 | 4.0 | 0.439 | 0.00264 |
| D | 71.6 | 21.2 | 2.4 | 4.8 | 0.485 | 0.00171 |
| C | 68.0 | 25.1 | 2.6 | 4.3 | 0.495 | 0.00158 |
| H | 79.7 | 16.4 | 2.1 | 2.8 | 0.458 | 0.00235 |
| J | 84.0 | 14.0 | 1.0 | 1.0 | 0.476 | 0.00137 |
| K | 76.7 | 18.0 | 3.1 | 2.2 | 0.505 | 0.00124 |

analyzer. However, the photographs shown in Fig. 10A–C are SEM images of the polished and unetched surface of the weld cross section showing the presence of inclusions. The measured size (average diameter) and volume fraction of inclusions are as listed in Table 6 and graphically shown in Fig. 11A–C. There is a distribution of inclusion sizes. Further details on inclusion distribution will be discussed in a subsequent paper primarily focusing on the aspects of weld metal inclusions. The term 3-D means inclusion analysis done in three dimensions, i.e., volumetric. It is well known formation of intragranular acicular ferrite crucially depends on the presence of an optimum amount of inclusions. It is seen from the figures the inclusion content significantly differs in welds made under isoheat input conditions but with different combinations of current and speed.

## Discussion

It is well established (Refs. 5–8) that the toughness of ferrous welds is dependent on the presence of a microstructure predominantly consisting of intragranularly formed acicular ferrite (AF). This is because of a basket-weave-type morphology, 1–3 μ in size, with high angle boundaries and random orientation. This morphology makes the AF inherently resistant to crack propagation (Ref. 8) and to have low transition temperature values. On the other hand, presence of large proportions of upper bainite, ferrite side plates, or grain boundary ferrite are considered to be detrimental to toughness. These structures provide easy crack propagation paths, especially when continuous films of carbides are present between ferrite laths or plates.

The final microstructure developed as a result of welding is principally governed by the relative position of the continuous cooling transformation (CCT) diagram for the particular weld metal and the actual weld cooling curve. The position of the CCT curve will depend on the carbon content, percentage of hardenability elements, prior $\gamma$ grain size, and the presence of inclusions. It should be noted, in general, the role of hardenability elements is to delay the transformation (shift the CCT curve to the right). On the other hand, an increase in inclusions favors the transformation (shift the CCT curve to the left). The higher the prior austenite grain size, the more the CCT curve will be shifted toward the right and vice versa. For a given weld composition and cooling rate, the type of microstructure will essentially depend on the level of inclusions and prior $\gamma$ grain size. Thus, development of a weld microstructure is a result of complex interaction between the material being welded, its thickness, and different welding parameters, as schematically depicted in Fig. 12. It should be stressed the overall conditions required to obtain predominantly AF structure lie in between those that promote martensite and bainite type of transformation (faster rate of cooling and shifting of cooling CCT curve to longer periods) and those that promote formation of $\alpha$ (slower cooling rate and shorter periods). It is apparent conditions

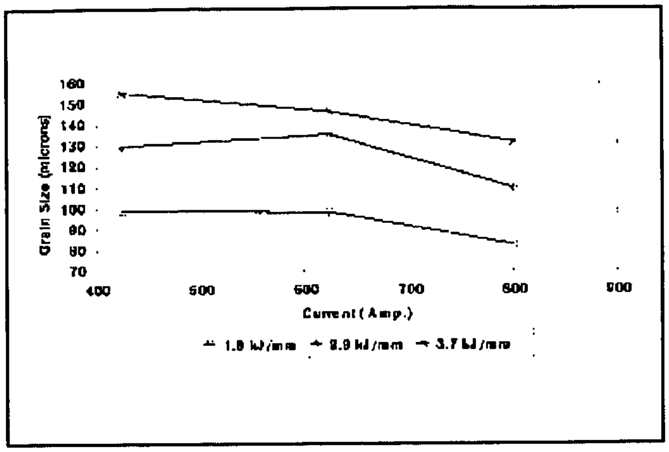

*Fig. 6 — Variation of prior austenitic grain size with current under isoheat input conditions.*

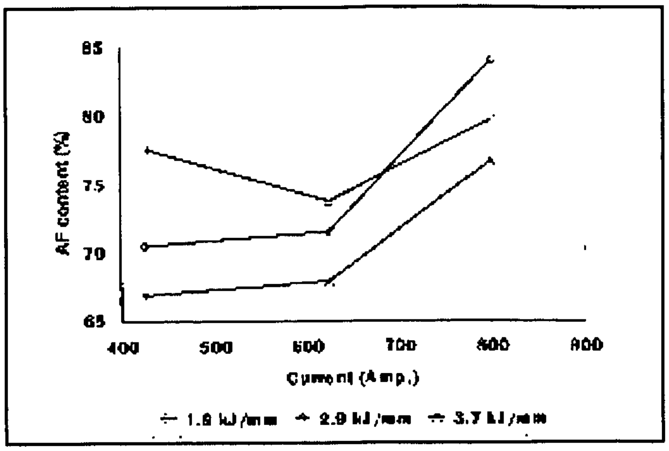

*Fig. 8 — Variation of acicular ferrite content with current under isoheat input conditions.*

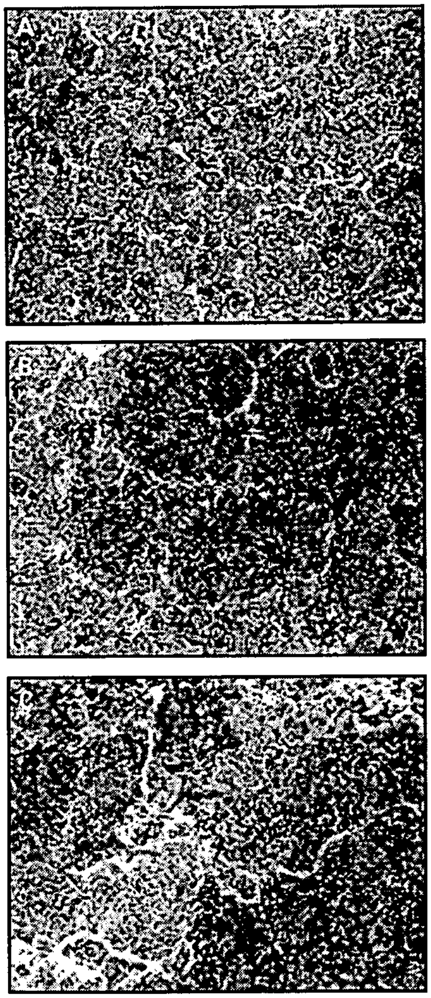

*Fig. 7 — Micrographs showing prior austenite grains. A — Weld H (100X); B — Weld C (100X); C — Weld G (63X).*

**Table 7 — Interdependency of Factors**

| | NA/Cl Ratio | Prior γ Grain Size, g (mm) | Inclusion vol. fr., f (%) | Inclusion Size, dv (μ) |
|---|---|---|---|---|
| NA/Cl ratio ↑ | — | ↑ | ↓ | ↑ |
| Prior γ Grain Size ↑ g (mm) | — | — | ↓ | ↑ |
| Inclusion vol. fr., ↑ f (%) | — | ↓ | — | — |
| Inclusion Size, ↑ dv (μ) | — | ↑ | — | — |

for maximizing AF require optimization of various interrelated parameters.

In the present case, variation in the weld compositions obtained during various welding trials was not significant (dilution varied between 50 and 60%) except in the case of carbon content. The minimum carbon content was 0.054% (Weld G) and maximum 0.077% (Weld E). However, for most of the welds, carbon content was between 0.063 and 0.075%. An increase in carbon content is known to shift the CCT curve to longer times. However, this effect has not been considered significant as compared to other parameters because the differences in the carbon contents of the welds are not very large, especially in view of the presence of other alloying elements that contribute to hardenability. Thus, the CCT curve, as far as the role of hardenability elements are concerned, can reasonably be assumed to be fixed. Hence, one needs to essentially consider the prior austenite grain size and the volume fraction of inclusions found in different welds, both of which showed substantial variations in different welds (Tables 5, 6).

Last, but not least, the actual cooling rate experienced by the weld should be considered. It is important to know in studying the effect of welding parameters, for convenience' sake, the parameters are usually combined and expressed as heat input. This approach, although practical, may not reflect the individual effects of the various welding parameters, which could be significant and might vary under identical heat input conditions. This important aspect is clearly seen in Figs. 4–6, 8, and 11, wherein there is significant difference in the results (nugget parameters, γ grain size, etc.) obtained under identical heat inputs but with different welding current and speed combinations. This implies the cooling rate the weld experiences may not have a monotonic dependence on heat input, especially when the welding current is high.

From Fig. 4 and Table 5, it is clear with an increase in current there is an increase in NA. The NA will depend on penetration and the factors that tend to increase width and reinforcement. At the highest heat input, a sharp increase is also noted in NA when going from 425 to 625 A. However, from 625 to 800 A, the change is not significant. Thus, it is seen under constant heat input conditions a wide variation in nugget area is obtained and the variation increases as heat input is increased. Under these conditions, it is unrealistic to expect similar weld metal properties when the same heat input but different welding current and speed combinations are used.

### Dependence of Heat Extraction from FZ on the Weld Nugget Morphology

Empirical expressions for weld cooling

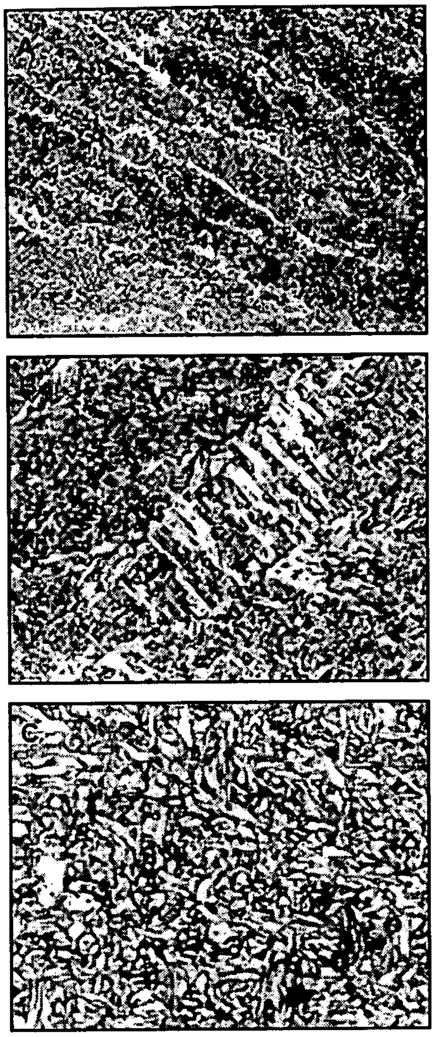

*Fig. 9 — A — Micrograph showing GBF in Weld E (250X); B — micrograph showing FSP in Weld G (500X); C — micrograph showing AF in Weld J (1000X).*

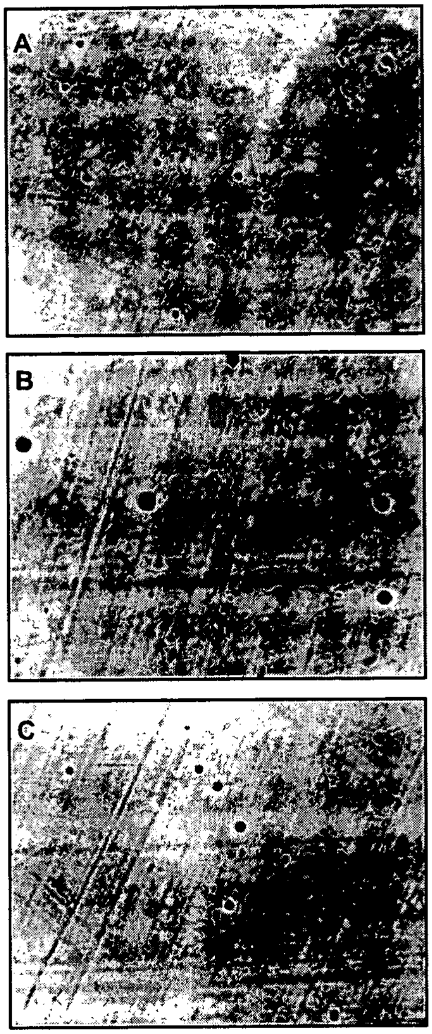

*Fig. 10 — Micrographs showing weld metal inclusions. A — Weld I (3000X); B — Weld G (3000X); C — Weld K (3000X).*

rate available as thick and thin plate solutions (Refs. 9, 11) do not take into account the effect of the wide variety of nugget morphologies obtainable under the same heat input but with different welding speed and current combinations. These solutions do not agree with the actual weld cooling rates measured (Ref. 12). A simple approach is presented here introducing the concept of NA/C1 ratio (Ref. 13). In the conventional approach, the cooling rate is qualitatively thought to be directly proportional to the effective plate thickness and inversely proportional to the heat input. In the present approach, the cooling rate the weld actually experiences is thought to be related to NA/C1. With increasing current at constant heat input, welding speed is required to be increased proportionately. This leads to an increase in the dimensionless operating parameter, $n$, given by $n = HI \times v^2/k$; where $k$ is a material-related constant involving thermophysical constant properties (Ref. 14). It is established that, with increasing $n$, weld NA increases. Obviously, melting efficiency will increase for the same heat input. Note the operating parameter is proportional to the square of the welding speed at any given heat input.

As defined earlier, nugget area (NA) quantitatively represents the amount of heat required to be dissipated by the surrounding substrate metal and will depend on heat input in the conventional sense. C1, on the other hand, represents the FZ/HAZ interface available for conducting away the heat that accumulates in the fusion zone. For cooling rate estimation, it is common practice to evaluate effective plate thickness, heat input, thermal diffusivity of the material, and joint geometry. Based on the value of this effective plate thickness, it is assumed the heat transfer in 2-D or 3-D and approximate solutions are used to estimate the cooling rate experienced by the weld. In the present approach, the ratio NA/C1 is proposed to represent the cooling rate. Exclusions of thermophysical properties in this relationship are justified because the same material is being considered in all the welds.

The relationship is not expected to be linear but, with the assumptions made in defining NA and C1, it can be stated the greater the ratio, the lesser the cooling rate and vice versa. The positive feature of this approach is inclusion of the morphological feature of the weld nugget resulting from the particular combinations of welding parameters, which is not possible in the conventional approach (Refs. 13, 15). A plot of NA/C1 vs. current at various heat inputs is shown in Fig. 13. It is clearly unreasonable to expect identical cooling rates for welds prepared with the same heat input but different current and speed combinations.

### Maximization of Acicular Ferrite in Microstructure

Development of a weld microstructure consisting predominantly of intragranularly formed acicular ferrite (75% or more) (Ref. 16) has always been the aim when welding carbon and low-alloy steels. It is generally accepted (Ref. 17) achievement of the above depends on favorable disposition of interdependent factors such as the following: prior austenite grain size, presence of optimum volume fraction of potent nucleation sites such as inclusions 0.2–0.5 $\mu$ in size, fusion zone chemistry with respect to hardenability elements, and cooling rate actually experienced by the weld. On cooling, the austenite transforms to a variety of micromorphologies as follows (approximate transformation starting temperatures are in parentheses): grain boundary ferrite (~800°C), ferrite side plates (~750°C), polygonal ferrite (~750–650°C), and acicular ferrite (~650°C) (Ref. 7). In addition, a variety of residual phases (Ref. 18), referred to as microphases, consisting of small amounts of martensite, retained austenite, and degenerate pearlite, also form. Usually the transformation to ferrite morphologies is quite efficient and the total amount of residual phases not significant. Since cooling is continuous, the final microstructure will contain many of the previously mentioned phases with the volume percent distribution of each phase decided by the particular combination of interrelated factors mentioned earlier that exist during welding. As suggested in a recent work (Ref. 19), it is useful to visualize a small region in the weld CCT diagram called the acicular ferrite window. If the actual weld cooling curve passes through the fair portion of this window, then acicular ferrite will be maximized. The position of this window will be decided by the first three factors mentioned earlier — Fig. 14. It should be remembered Fig. 14 is just a schematic

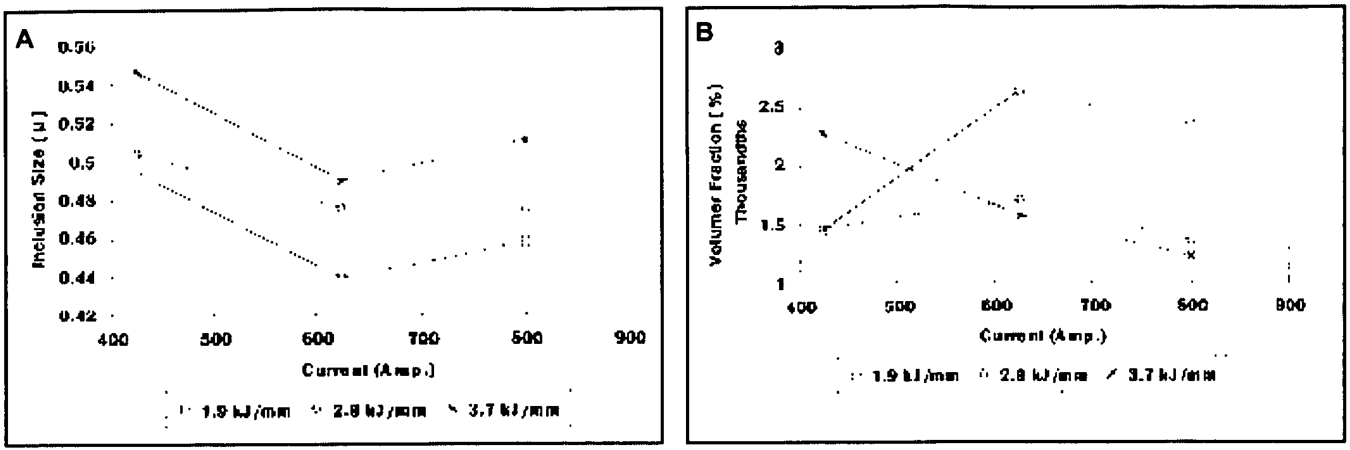

*Fig. 11 — A —Variation of inclusion size with current under isoheat input conditions; B — variation of inclusion volume fraction with current under isoheat input conditions.*

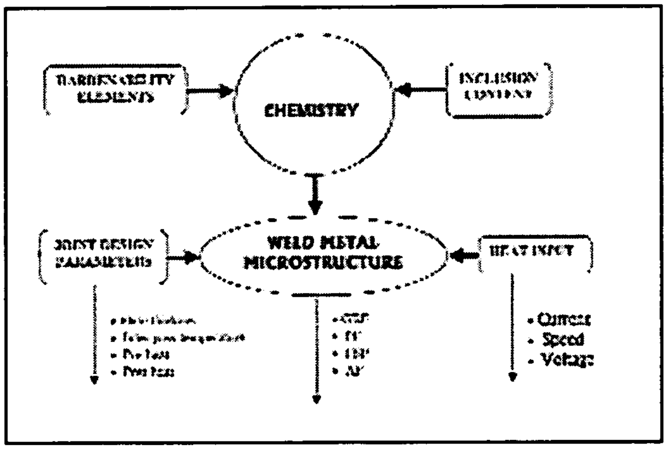

*Fig. 12 — The various factors that play a role in deciding weld microstructure.*

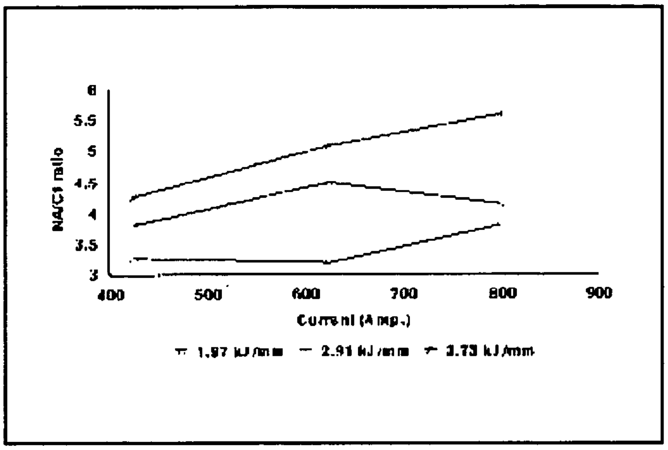

*Fig. 13 — Plot of NA/C1 ratio with current under isoheat input conditions.*

representation of an ideal situation. The key to maximizing acicular ferrite is for the actual weld cooling rate to avoid the FSP formation zone as far as possible. This is because once FSP is nucleated, it grows at a rapid rate with the growth terminating on soft impingement with other FSP by acicular ferrite. Since all these factors are related to the welding parameters, in principle it should be possible to determine, for a given set of conditions, optimum parameter settings for maximizing acicular ferrite. However, it is essential to first obtain correlation between factors that are responsible for the metallurgical phenomena leading to acicular ferrite formation.

### Prior Austenite Grain Size (g)

It is well established (Refs. 20–22) that a minimum prior austenite grain size is required below which formation of acicular ferrite is not favored. The primary reason is the greater availability of grain boundary nucleation and growth sites for the high-temperature diffusional transformation products, i.e., GBF. By the time the kinetics of these reactions slow down parabolically, limited nontransformed austenite is available for the low-temperature displacive process of forming acicular ferrite leading to an inadequate volume fraction of the desirable phase (Ref. 6). As the grain size increases, formation of acicular ferrite is encouraged, provided other factors are favorable. However, above a particular grain size, formation of AF is discouraged due to shifting of the CCT curve to longer times leading to lower temperature transformation products such as bainite and martensite (Ref. 16). The available information suggests an optimum size; however, that would depend on other factors. It has been reported for a certain weld chemistry (low Ti-B welds of low C steels), optimum values lie in the range of 20–60 $\mu$ (Ref. 17). From Fig. 6, it is clear prior austenite grain sizes can be significantly different under the same heat input but with different current and speed combinations. This is more pronounced at higher heat inputs. It should also be remembered the size would also depend on the cooling rate represented by NA/C1 and inclusion volume fraction. Lower values of the former and higher values of the latter should lead to smaller grain size. Under isoheat input conditions (Fig. 6), the prior $\gamma$ grain size decreased with an increase in current level. This indicated for welds made with identical heat inputs but different combinations of welding current and speed, the resultant microstructures may not be the same because the prior $\gamma$ grain size influences the microstructural transformation to a great extent. This will definitely have its effect, in turn, on the final mechanical properties of the weld metal.

### Volume Fraction of Inclusions

It is well established (Ref. 17) that presence of an adequate amount of inclusions of sizes greater than 0.25 $\mu$ is necessary to allow the intragranular formation of acicular ferrite. Controversy exists (Refs. 22, 23) as to whether the potency of these inclusions depends on their chemical nature or whether they merely provide inert surfaces to enable the nucleation of the acicular ferrite. However, the following are clear as far as the role of these inclusions:

a) There is no possibility of obtaining any acicular ferrite in the absence of inclusions.

b) The inclusion size should be in the range of 0.25 to 0.50 microns.

c) Inclusions at the grain boundaries have a dual role to play, i.e., smaller ones

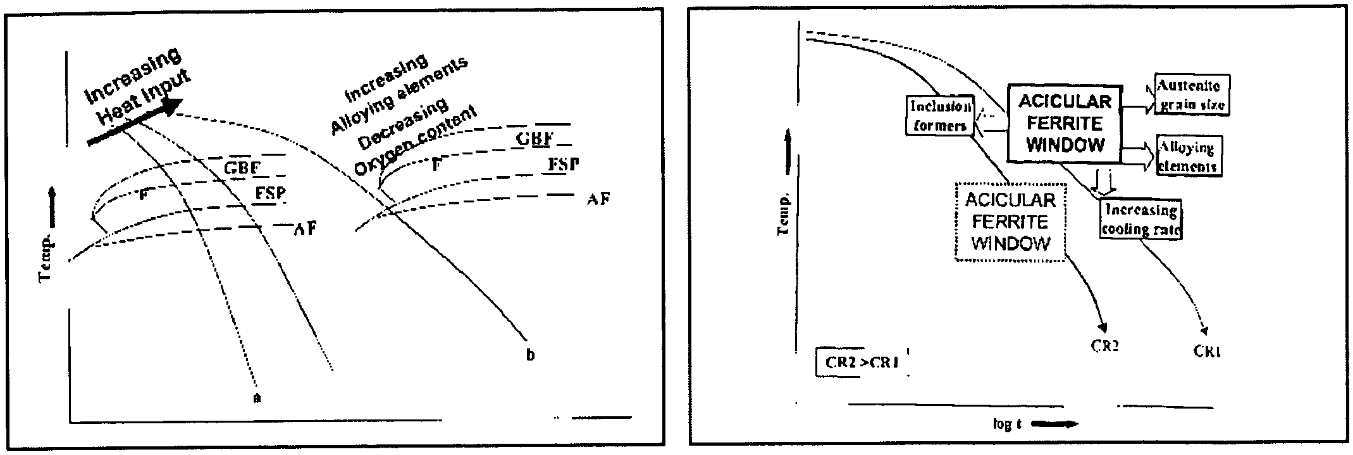

*Fig. 14 — Schematic showing the position of the acicular ferrite window and CCT diagram with respect to alloying elements, austenite grain size, and cooling rate.*

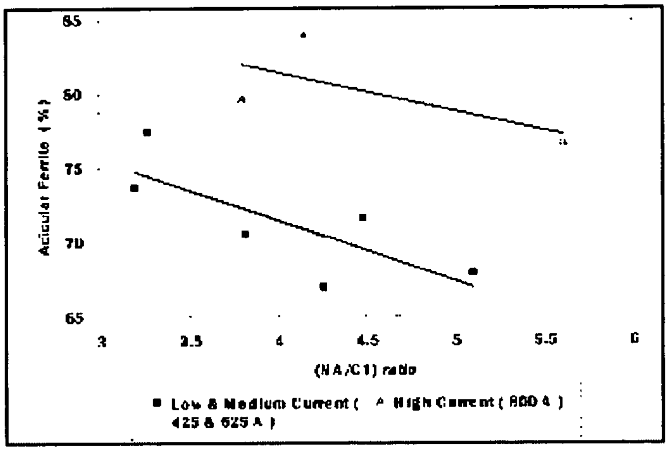

*Fig. 15 — Variation of acicular ferrite content with NA/C1 ratio.*

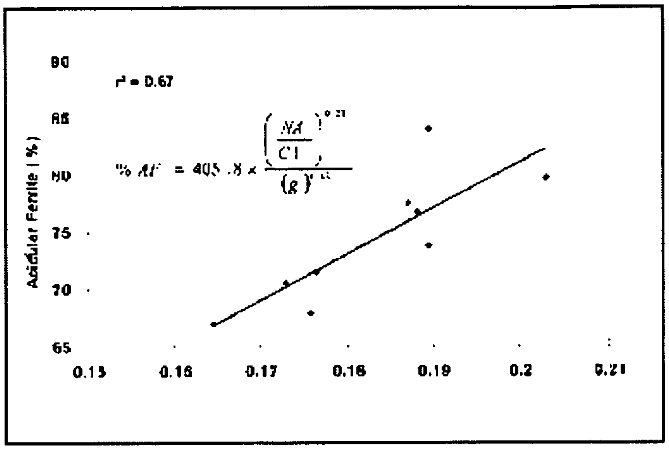

*Fig. 16 — Correlation of acicular ferrite content with NA/C1 ratio and prior austenitic grain size.*

restrict grain growth and larger ones encourage nonacicular ferrite transformations (both these events are detrimental to the final microstructure formed).

d) The above leads to an upper limit to the desired volume fraction of inclusions.

e) The greater the volume fraction (less than the upper limit), the smaller the interinclusion distances will be and the finer the acicular ferrite plates.

f) Several plates of acicular ferrite can form per inclusion.

As in the case of other metallurgical factors, inclusion characteristics, namely, inclusion size and volume fraction, significantly depend on the welding current and speed combinations used even though carried out at same heat input (see, respectively, Figs. 11A, B). It is seen from these figures and Table 4 there exists some correlation between oxygen content in the weld and inclusion volume fraction, especially at medium and higher heat inputs.

## Cooling Rate

Weld cooling rate plays the decisive role in determining weld microstructure. The general effect of increasing the cooling rate is to lower transformation temperatures. When cooled at sufficiently low rates, the microstructure predominantly tends to become polygonal ferrite-pearlite. As the cooling rate is progressively increased, there is a tendency for the polygonal ferrite to be refined and become limited to the prior austenite grain boundaries (Ref. 24). This morphology is often referred to as grain boundary allotriomorphs. Increased cooling rates also reduce, and eventually eliminate, the pearlite phase. The weld microstructure can also show Widmanstatten side plate morphologies that grow out of the large polygonal ferrite grains at low cooling rates or out of the grain boundary allotriomorphs at higher cooling rates. An increased cooling rate tends to increase the ratio of side plates to polygonal ferrite in the final microstructure. It is useful to remember kinetics of side plate growth, which is a displacive phenomena and relies on the instability of the austenite/ferrite interface, is extremely fast as compared to the diffusion-limited parabolic growth rate of grain boundary ferrites. At intermediate cooling rates, provided inclusions are present, intragranular formation of acicular ferrite is encouraged. At still higher cooling rates, the lath ferrite structure, consisting of colonies of parallel laths of ferrite separated by retained austenite or carbides, dominates. Finally, at the highest cooling rates, depending upon the hardenability elements, lath martensite is formed.

Recall, in the present work, cooling rate is represented by NA/C1 and, from Fig. 15, it is clear, at the same heat input, obtaining significantly different microstructure is possible depending upon the welding current and speed combination.

## Interdependency of the Factors

It is useful to discuss the interdependency between the three factors discussed previously. It should be noted fusion zone chemistry has not been discussed because it is assumed, since there has not been sig-

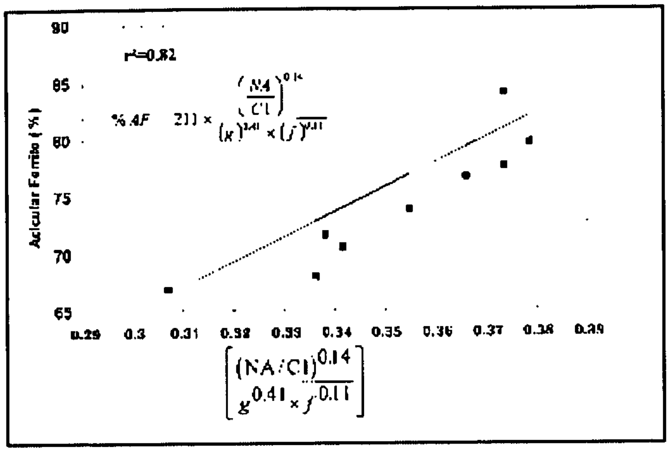

Fig. 17 — *Correlation of acicular ferrite content as a function of NA/C1 ratio, prior austenitic grain size, and inclusion volume fraction.*

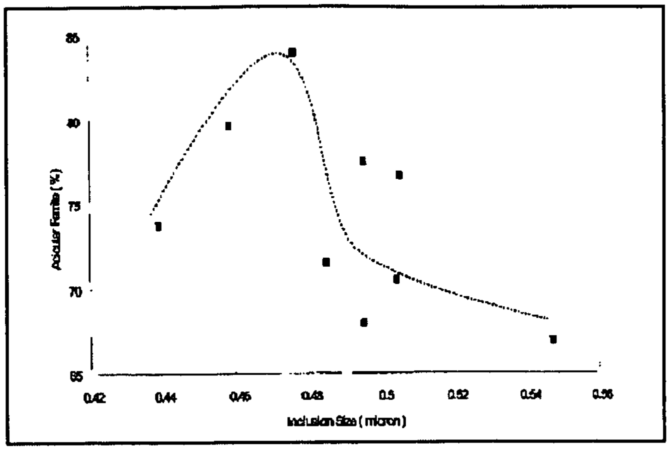

Fig. 18 — *Variation of acicular ferrite content with mean inclusion size.*

nificant variation in them, with the limited experimental data generated, the discussion will be of a qualitative nature based on basic principles of the welding process. Table 7 shows the matrix of the factors discussed and indicates how each can influence the other.

For higher NA/C1, cooling is slower so the weld will spend a longer time at higher temperatures, leading to larger austenite grain size. At the same time, there will be greater chance for the inclusions to be absorbed by the slag leading to a drop in the volume fraction of inclusions. Furthermore, the average size of the inclusion is likely to be larger. It is unlikely prior austenite grain size is likely to influence the other factors. With respect to inclusion parameters, greater volume fraction will lead to a greater presence of inclusions at the grain boundaries, some of which can act as grain pinning agents and lead to reduction in grain size. As the inclusion size increases, prior austenite grain size will tend to increase because of lesser pinning potential. It is clear from the previous qualitative statements, the cooling rate represented by NA/C1 will have a dominant role to play in deciding the nature of weld microstructure as it appears to affect all the other factors affecting the ultimate weld microstructures.

**Dependence of Correlation between Different Factors Responsible for the Formation of Acicular Ferrite**

Since NA/C1 appears to play a dominant role in deciding the microstructure, the percentage of acicular ferrite as a function of NA/C1 was plotted as in Fig. 15. It was found necessary to fit the data points corresponding to higher current separately from the data points corresponding to low and medium currents. The figure also shows, for similar cooling conditions, a higher volume fraction of AF is obtained at high currents. This could be related to the fact at higher currents the weld pool is subjected to significantly greater convective flow since the contribution by electromagnetic stirring effects is larger. This can have an effect on the inclusion characteristics leading to different microstructures.

To remove the above separation, other factors, namely, prior austenite grain size (g) and volume fraction of inclusions, were incorporated one by one. The first correlation (Fig. 16) was obtained by performing regression analysis between the percentage of acicular ferrite and the combination of NA/C1 and g. The following correlation was then obtained:

$$\%AF = 405.8 \times \frac{\left(\frac{NA}{C1}\right)^{0.23}}{(g)^{0.43}} \qquad (1)$$

The correlation was not a good one since r² was only 0.67. An improvement to r² = 0.82 was observed by including the volume fraction of inclusions (f) — Fig. 17. The improved relationship was

$$\%AF = 211 \times \frac{\left(\frac{NA}{C1}\right)^{0.14}}{(g)^{0.41} \times (f)^{0.11}} \qquad (2)$$

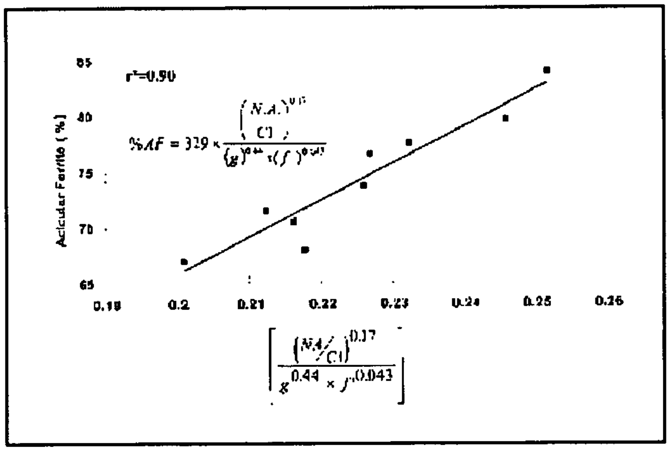

Fig. 19 — *Correlation of acicular ferrite content with NA/C1 ratio, austenite grain size (g), and modified volume fraction of inclusions (f').*

To further improve the correlation, help was taken from the fact there is a critical range of inclusion size that is likely to be most potent (Ref. 25). From Fig. 18, it can be seen volume fraction of AF is maximized when the sizes of the inclusions are within a range of 0.44 to 0.5 μ. On performing regression analysis between *%AF* and the combination of *NA/C1*, *g*, and $f^{l}$ represent the modified volume fraction of inclusions (only inclusions between 0.44 and 0.5 μ were considered), a higher r² value of 0.90 was obtained — Fig. 19. The ultimate relationship obtained was

$$\%AF = 329 \times \frac{\left(\frac{NA}{C1}\right)^{0.17}}{(g)^{0.44} \times \left(f^{1}\right)^{0.043}} \qquad (3)$$

The correlation shown in Equation 3 appears to be reasonably acceptable considering the complexity of the processes involved. The practical utility of the correlation can only be realized when the same can be represented in terms of welding parameters. Each of the terms appearing in Equation 3 has been correlated with welding current and speed (Ref. 13). It was then possible to correlate the AF content with welding parameters. That will form the subject of a subsequent paper. The utility of this correlation for setting up the practical welding parameters appears to be restricted as it involves sectioning of the weld. However, this correlation can serve the purpose of giving starting welding parameters for similar grades of steel substrates and consumables. The magnitude of exponents of the various terms in Equation 3 are possibly indicative of the allowable tolerance of the three main factors responsible for obtaining a given level of AF content in the weld microstructure. Prior austenite grain size appears to be most critical as indicated by a relatively high value of exponent 0.44 as compared to other exponents. A very small value for the exponent on inclusion volume fraction (0.043) does not mean that without the inclusion it is possible to obtain any intragranularly formed AF. All it possibly means is a wide range of inclusion content is acceptable to get the desired AF content in the weld microstructure.

## Conclusions

From the present investigation, it is seen significant variations in bead morphology and weld microstructure can occur under identical heat input but with different current and travel speed combinations. From the present investigation, the following major conclusions can be made.

1) Depending upon the welding current and travel speed combinations used, significantly different dependence of all the influencing parameters were observed even though heat input was the same. This can be attributed to differences in the weld bead morphologies. Different weld bead morphologies are likely to lead to different weld cooling rates that will affect the microstructure by itself and also different microstructural features, e.g., austenite grain size, inclusion parameters, that, in turn, will further contribute to the final AF content.

2) A new cooling parameter NA/C1 was found to be a useful representation of the actual weld cooling rate. Rosenthal's work on moving heat source allows expression of the cooling rate based on quantities that can be measured/determined prior to welding (plate thickness, heat input, preheat, etc.). But it need not necessarily represent the true cooling rate because of the empirical nature of defining the heat transfer situation and also in not taking cognizance of the actual bead morphology that forms.

3) Using multiple regression analysis along with other interdependent factors, a correlation between acicular ferrite and the influencing parameters was obtained with a high degree of correlation coefficient. From the magnitude of the exponents of the various terms in the correlation derived, it appears prior austenite grain size is the most critical factor. On the other hand, the low value of the exponent on inclusion volume fraction suggests that, although necessary, some variations in the inclusion volume fraction can be tolerated to obtain a desirable AF content. The magnitude of the exponent on factor NA/C1, which represents the true cooling rate, is intermediate and indicative of greater tolerance than that allowed for prior austenite grain size.

4) The correlation has been derived on the basis of sectioning of the welds. However, the correlation can serve the purpose of obtaining starting welding parameters for similar grades of steel substrates and consumables. For this it is necessary to establish the correlation between various factors and welding parameters (Ref. 13).

5) The full utility of this correlation derived for the present combination of steel substrates and consumables can be realized if realistic mathematical modeling of weld bead morphology, i.e., NA/C1 ratio and microstructural features like prior austenite grain size and inclusion volume fraction can be performed.

### *References*

1. Dixon, B., and Hakansson, K. 1995. Effect of welding parameters on weld zone toughness and hardness in 690 MPa steel. *Welding Journal* 64(4): 122-s.

2. Oldland, P. T., Ramsay, C. W., Matlock, D. K., and Olson, D. L. 1989. Significant features of high-strength steel weld metal microstructures. *Welding Journal* 58(4): 158-s.

3. Smith, N. J., McGrath, J. T., Gianetto, J. A., and Orr, R. F. 1989. Microstructures/mechanical property relationships of submerged arc welds in HSLA 80 steels. *Welding Journal* 58(3): 112-s.

4. Gianetto, J. A., Smith, N. J., McGrath, J. T., and Bowker, J. T. 1992. Effect of composition and energy input on structure and properties of high-strength weld metals. *Welding Journal* 61(11): 407-s.

5. Farrar, R. A., and Zhang, Z. 1995. Aspect ratios and morphology of acicular ferrite in C-Mn-Ni weld metals. *Materials Science Technology* 11: 759.

6. Ricks, R. A., Howell, P. R., and Barritte, G. S. 1982. Nature of acicular ferrite in HSLA steel weld metal. *Journal of Materials Science* 17: 732.

7. Abson, D. J., and Dolby, R. E. 1978. *Weld Inst. Res. Bull.* 19: 202–207,

8. Bhadeshia, H. K. D. H. 1990. *Proc. Conf. on the Metallurgy, Welding and Qualification of Microalloyed (HSLA) Steel Weldments.* Houston, Tex., pp. 34–69.

9. Rosenthal, D. 1941. Mathematical theory of heat distribution during welding and cutting. *Welding Journal* 20(5): 220-s to 234-s.

10. Abson, D. J., and Pargeter, R. J. 1986. Factors influencing as-deposited strength, microstructure and toughness of manual metal arc welds suitable for C-Mn steel fabricators. *International Metals Review* 31(4): 141–194.

11. Easterling, K. 1992. *Introduction to Physical Metallurgy of Welding.* Butterworth-Heineman Ltd., p. 20.

12. Chakraborty, A. P., Thibau, R., and Bala, S. R. 1985. Cooling characteristics of bead-on-plate welds. *Metal Construction* (3): 178 R.

13. Basu, B. 2000. Effect of welding parameters on the structure and properties of a submerged arc weld of a high-strength structural steel. Ph.D. dissertation. IIT – Bombay.

14. Messler, R. W. 1999. *Principles of Welding Processes — Physics, Chemistry and Metallurgy.* John Wiley & Sons Inc., A Wiley Interscience Publication., p. 167.

15. Basu, B., and Raman, R. 2000. Influence of weld bead morphologies on the structure and properties of submerged arc weld metal. Paper No. WM-21, *Symposium on Joining of Materials*, Tiruchirapalli, India.

16. Farrar, R. A., and Harrison, P. L. 1987. Acicular ferrite in carbon-manganese weld metals: An overview. *Journal of Mater. Sci.* 22(11): 3812.

17. Thewlis, G. 1994. Transformation kinetics of ferrous weld metal. *Mater. Science Tech.* 2: 110–125.

18. Honeycombe, Sir. R., and Bhadeshia H. K. D. H. 1995. *Steels — Microstructure and Properties*, p. 280. London, U.K.: Edward Arnold.

19. Yelpale, P. S. 2000. Influence of the presence of active gas in shielding gas mixture on weld quality. M. Tech. dissertation. IIT – Bombay.

20. Grong, O., and Matlock, D. K. 1986. Microstruture development in mild and low-alloy steel weld metals. *Int. Mater. Rev.* 31(1): 27.

21. Ferrante, M., and Farrar, R. A. 1982. The role of oxygen rich inclusions in determining the microstructure of weld metal deposits. *Journal of Mat. Sci.* 17: 3293.

22. Liu, S., and Olson, D. L. 1986. The role of inclusions in controlling HSLA steel weld metal microstructues. *Welding Journal* 55(6): 139-s.

23. Brooksbank, D., and Andrews, K. W. 1972. Stress fields around inclusions and their relation to mechanical properties. *Journal of the Iron and Steel Institute*, pp. 210–246.

24. Harrison, P., and Farrar, R. 1987. Microstructure and toughness of C-Mn and C-Mn-Ni weld metal — Part I. *Metals Construction* 7: 392R–399R.

25. Mills, A. R., Thewlis, G., and Whiteman, J. A. 1987. The nature of inclusions in steel weld metals and their influence on the formation of acicular ferrite. *Mater. Sci. Tech.* 3: 1051–1061.